

1 *For submission to Innovative Food Science and Emerging Technologies*

2 **A novel strategy for improving radio frequency heating uniformity of dry food**
3 **products using computational modelling**

4 Zhi Huang¹, Francesco Marra², Shaojin Wang^{1,3*}

5

6 ¹*College of Mechanical and Electronic Engineering, Northwest A&F University, Yangling,*
7 *Shaanxi 712100, China*

8 ²*Dipartimento di Ingegneria Industriale, Università degli studi di Salerno, Fisciano, SA, Italy*

9 ³*Department of Biological Systems Engineering, Washington State University, 213 L.J. Smith*
10 *Hall, Pullman, WA 99164-6120, USA*

11

12

13

14

15

16 *Corresponding author: Shaojin Wang, Ph.D, Professor. Tel.: +86-29 87092391; Fax: +86- 29
17 87091737; Email address: shaojinwang@nwsuaf.edu.cn

18

19 **Abstract**

20 This study attempted to quantify effects of dielectric properties (DPs) of a surrounding
21 container and treated food products on heating uniformity in a 6 kW, 27.12 MHz parallel plate
22 radio frequency (RF) system. A computer simulation model was established with finite
23 element-based commercial software, COMSOL Multiphysics[®], and experiments with 1.5 kg
24 soybean flour packed in a rectangular polystyrene container were performed to validate the
25 developed model. Surface temperature distributions of soybean flour in three different
26 horizontal layers were obtained with an infrared camera, and temperature-time histories at two
27 representative locations inside the container were monitored with two fiber optical sensors.
28 The uniformity index (UI) was used as criterion to evaluate RF heating uniformity within food
29 products. Results showed that the temperature uniformity of food samples was clearly
30 influenced by DPs and density of the surrounding container. UI was the lowest when the
31 surrounding container dielectric constant was in a comparable range of the sample's, with the
32 loss factor values of surrounding container lied between 0.01-0.1% of the sample's. The
33 optimum RF heating uniformity of food products could be achieved with a smaller density
34 value of the surrounding container. The correlations of DPs and density between surrounding
35 container and food products derived from the validated simulation model could provide
36 valuable information and strategy to improve the RF heating uniformity of low moisture
37 foods for insect or microbial control. Thus, the established strategy can further be used for
38 developing effective industrial-scale RF treatment protocols after optimization of this process
39 by the food industry.

40 **Keywords:** Computer simulation; Dielectric properties; Heating uniformity; Radio frequency;
41 Soybean flour.

42 **1. Introduction**

43 Low moisture foods, such as wheat flour, corn meal, glutinous rice flour, nuts, spices, and
44 milk powders, are normally considered as shelf stable foods and can be stored for a long time
45 due to preventing bacterial growth in its low moisture environment. Soybean flour is a
46 popular food due to its high nutritional value and functional characteristics, which contain
47 flavonoids, fiber and bioactive peptides (Hassan, 2013). Pathogens and insect pests, however,
48 are found to survive in a low moisture environment more easily for several months (Finn,
49 Hinton, McClure, Amézquita, Martins, & Fanning, 2013; Johnson, Wang, & Tang, 2010;
50 Mohapatra, Kar, & Giri, 2015). The qualitative and quantitative losses can be reached as high
51 as 30% due to insect damages (FAOSTAT, 2013), which also promote mold growth, toxin
52 production, and product degradation in low moisture foods (Jiao, Johnson, Tang, & Wang,
53 2012; Vijay, Bhuvaneshwari, & Gajendran, 2015). Several cases of soybean flour
54 contamination with *Plodia interpunctella* greatly affect the quality and taste properties of the
55 end product made by the flour (Singh, Satya, & Naik, 2013; Taylor, Fields, & Sutherland,
56 2007). Radio frequency (RF) heat treatment has been considered as a novel heating
57 technology for controlling insect and microbial populations in several dry products, such as
58 almond (Gao, Tang, Villa-Rojas, Wang, & Wang, 2011), date (Ben-Lalli, Bohuon, Collignan,
59 & Méot, 2013), lentil (Jiao et al., 2012; Wang, Yue, Chen, & Tang, 2008), peanut butter
60 cracker (Ha, Kim, Ryu, & Kang, 2013), raisin (Alfaifi et al., 2014), spice (Kim, Sagong, Choi,
61 Ryu, & Kang, 2012), walnut (Mitcham et al., 2004; Wang et al., 2008), and wheat (Shrestha,
62 & Baik, 2013).

63 Although the most important characteristic of RF treatments is fast and volumetric
64 heating generated by dipole rotation and ionic conduction, edge over-heating is still a major
65 problem for foods heated in rectangular containers (Frag, Marra, Lyng, Morgan, & Cronin,
66 2010; Tiwari, Wang, Tang, & Birla, 2011a,b; Alfaifi et al., 2014). Edges and corners always

67 absorb more electromagnetic energy compared to other regions due to different dielectric
68 properties (DPs) between food products and the surrounding media (usually air), resulting in
69 an uneven electric field distribution (Birla, Wang, Tang, & Hallman, 2004). The non-uniform
70 heating in RF treated products may cause either survivals of pathogens/insects or degraded
71 quality (Birla et al., 2004; Jiao et al., 2012; Geveke, Kozempel, Scullen, & Brunkhorst, 2002;
72 Kim et al., 2012; Kirmaci & Singh, 2012). A number of methods have been reported for
73 overcoming non-uniform RF heating, such as combining with an external heating or cooling
74 (Birla et al., 2004; Hou, Ling, & Wang, 2014; Liu, Wang, Mao, Tang, & Tiwari, 2013; Wang,
75 Tiwari, Jiao, Johnson, & Tang, 2010), enclosing in another medium (Ikediala, Hansen, Tang,
76 Drake, & Wang, 2002; Jiao, Tang, & Wang, 2014a; Luechapattanaporn et al., 2005), mixing
77 or rotating food (Birla et al., 2004; Chen, Wang, Li, & Wang, 2015a), modifying electrode
78 shapes (Tiwari et al., 2011a; Alfaifi et al., 2014), and sample movement (Chen, Huang, Wang,
79 Li, & Wang, 2015b; Wang, Monzon, Johnson, Mitcham, & Tang, 2007). The trial and error
80 procedures are time consuming, costly, and often provide limited information, which cannot
81 easily identify the mechanism behind non-uniform RF heating. Finite element modelling may
82 serve as valuable tools to acquire deep insights on the heating uniformity of products and
83 offer opportunity to clearly understand RF interactions with food components without the
84 necessity of extensive experiments.

85 Modeling RF processes is a multi-physics problem that involves the solution of coupled
86 electromagnetic and heat transfer equations. Several simulation models have been developed
87 to improve the RF heating uniformity for different food materials, such as apple (Birla et al.,
88 2004), fish (Llave, Liu, Fukuoka, & Sakai, 2015), meat batters (Marra, Lyng, Romano, &
89 McKenna, 2007), peanut butter (Jiao, Shi, Tang, Li, & Wang, 2015b), raisins (Alfaifi, et al.,
90 2014), shell eggs (Lau, 2015), soybeans (Huang, Zhu, Yan, & Wang, 2015c), wheat flour
91 (Tiwari et al., 2011a,b), and wheat kernels (Jiao, Deng, Zhong, Wang, & Zhao, 2015a). The

92 simulated uniformity index (UI) has been used as criteria to evaluate the temperature
93 uniformity in RF treated products (Alfaifi et al., 2014; Huang et al., 2015c; Jiao et al., 2015a;
94 Tiwari et al., 2011a; Wang, Yue, Tang, & Chen, 2005). Simulated results show that the RF
95 heating uniformity could be improved by immersing the model fruit in water, suggesting that
96 the non-uniform heating is mainly caused by the difference between DPs of food and its
97 surrounding medium (Birla et al., 2004; Huang, Zhang, Marra, & Wang, 2016; Jiao, Tang,
98 Wang, & Koral, 2014b). When the dielectric constant of surrounding material is in a
99 comparable range with the sample, the best heating uniformity would be achieved (Tiwari et
100 al., 2011a; Huang et al., 2015c). The dielectric constant determines the electric field
101 distribution when the loss factor is far smaller than the dielectric constant (Jiao et al., 2014a,b;
102 Metaxas, 1996). Surrounding the container with a more or less thick material, characterized
103 by dielectric constant similar to that of processed samples, provides better RF heating
104 uniformity (Huang et al., 2015c). Following this approach, Jiao et al. (2015b) have shown that
105 the temperature uniformity in peanut butter has been improved by minimizing the difference
106 of dielectric constant between food sample and surrounding material. However, there was no
107 available mathematical modelling in literature to identify the specific relationship of DPs
108 between surrounding material and treated products for RF heating uniformity improvement.
109 Therefore, it is desirable to conduct a numerical analysis to systematically study the RF
110 heating characteristics and design treatment protocols to improve RF heating uniformity in
111 low moisture foods.

112 The objectives of the current study were to: (1) develop a computer simulation model to
113 predict the electric field intensity and temperature distribution in three different layers of
114 soybean flour in a rectangular shaped container, (2) conduct experiments with soybeans flour
115 in a 6 kW, 27.12 MHz RF system to verify the simulation results, (3) apply the validated
116 model to evaluate the heating uniformity of soybean flour influenced by DPs and density of

117 the surrounding container and treated products, and (4) establish the DPs and density
118 correlations between surrounding container and treated food sample when the best heating
119 uniformity was obtained.

120 **2. Materials and methods**

121 2.1. Raw material preparation

122 Soybean flour (*Glycine max.*) was purchased from a local market in Yangling, Shaanxi,
123 China. A total of 20 kg of soybean flour were kept in polyethylene bags and stored at the
124 constant temperature (20 °C) in a thermostatic and humidity controlled chamber (BSC-150,
125 Shanghai BoXun Industrial & Commerce Co., Ltd., Shanghai, China). They were taken out
126 from the chamber and kept at ambient room temperature (20 ± 1 °C) for 4 h prior to RF
127 processing. The initial moisture content of tested soybean flour was 7.93 ± 0.08 % on wet
128 basis (w.b.). The chemical compositions of the flour were measured in the College of Food
129 Science and Engineering, Northwest A&F University, Yangling, China. The measurements
130 were made in three replicates and the standard methods used for each measurement are
131 summarized in Table 1.

132 Table 1. Compositions and measurement methods for soybean flour.

Composition		Method
Ash (g/100 g)	4.62	AOAC 920.181
Moisture (g/100 g w.b.)	7.93	AOAC 934.01
Fat (g/100 g)	18.26	AOAC 992.06
Protein (g/100 g)	32.64	AOAC 955.04
Carbohydrate (g/100 g)	30.61	CFR 101.9
Calories (Kcal/100 g)	418	CFR 101.9
Dietary fibre (g/100 g)	5.94	AOAC 994.13

133

134 2.2. Container material and dimensions

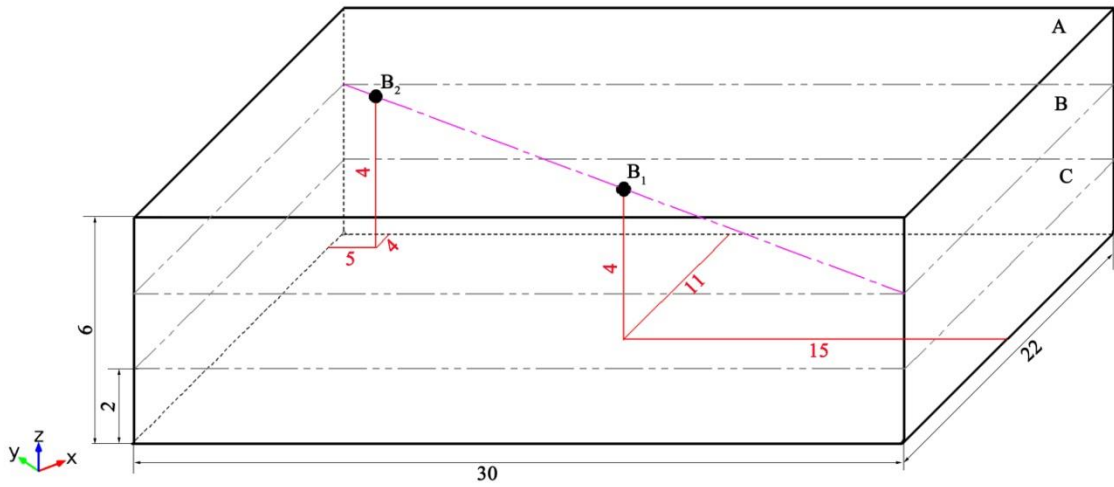
135 The polystyrene container was chosen based on the closest dielectric constant to that of
136 soybean flour with a small dielectric loss factor (Table 2). With the main advantage of lower
137 density, cheap, stable, high heat resistance and portable characteristics, polystyrene was
138 widely used in food processing and packaging industry. The inner dimension of the
139 rectangular polystyrene container was $30 \times 22 \times 6 \text{ cm}^3$, the thickness for the bottom and side
140 walls was fixed at 2 cm (Huang et al., 2016).

141

142 2.3. Temperature measurements

143 About 1.5 kg soybean flour samples filled the rectangular container were horizontally
144 divided into three layers (A: $z = 6 \text{ cm}$; B: $z = 4 \text{ cm}$; C: $z = 2 \text{ cm}$) parallel to the container
145 bottom by two thin polypropylene films (mesh opening of 0.2 mm) with each filled of 0.5 kg
146 to represent the temperature distribution inside the sample (Fig. 1). An infrared camera
147 (DM63-S, DaLi Science and Technology Co., LTD, Zhejiang, China) with an accuracy of \pm
148 $2 \text{ }^\circ\text{C}$ was used for mapping surface temperatures of soybean flour in three different layers
149 after RF treatment. The thermal digital infrared camera was first calibrated against a thin
150 thermocouple thermometer (HH-25TC, Type-T, OMEGA Engineering Inc., Stamford,
151 Connecticut, USA) with an accuracy of $\pm 0.5 \text{ }^\circ\text{C}$ and 0.9 s response time. For internal
152 temperature monitoring during RF heating, two optical fiber sensors (1.8 mm diameter)
153 attached to a temperature measurement system (FTS-P104, Xi'an HeQi Opo-Electronic
154 Technology Co., LTD, Shaanxi, China) were inserted at the center (B_1) and near the corner
155 (B_2) at middle layer ($z = 4 \text{ cm}$) of food sample. The optical fiber sensors were calibrated by
156 using ice-water mixture and boiling water before experiment and temperatures were recorded
157 at 1 s intervals. A plastic foam board ($29 \times 21 \times 2 \text{ cm}^3$) made from polystyrene was used to
158 cover on the top of the container. The sensors were inserted at the center (B_1) and corner (B_2)
159 of the board using a drill to ensure precise hole positioning (Fig. 1). These positions were held

160 by fixing the sensor cables to a stationary position through the feeding inlet of the RF
161 machine.



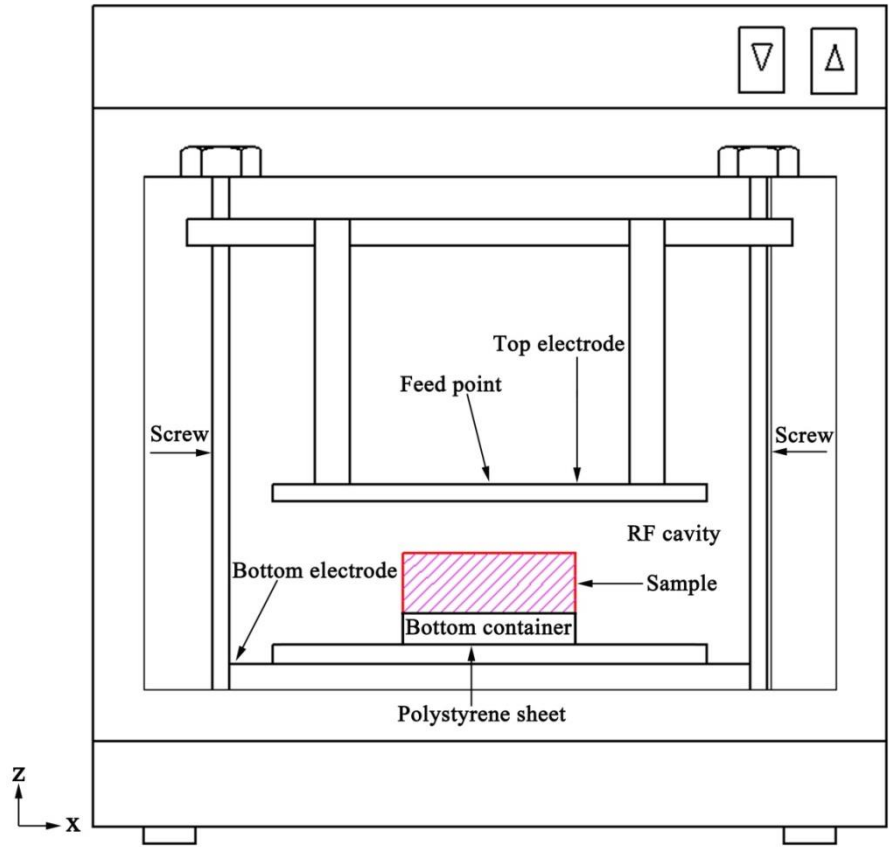
162
163 Fig. 1. Position of two fiber optical temperature sensors in the rectangular polystyrene
164 container split into three layers (A-top, B-middle, C-bottom layer) for temperature profile
165 measurements (all measures in cm).

166 2.4. Computer modeling of RF heating

167 2.4.1. Physical model

168 A 6 kW, 27.12 MHz free running oscillator pilot scale RF system (COMBI 6-S,
169 Strayfield International Limited, Wokingham, UK) was used in this study (inner dimension
170 $129 \times 109 \times 52 \text{ cm}^3$). This system consisted of a chamber with electrically insulated walls and
171 two parallel rectangular electrodes, a generator, power amplifier, matching unit, and a RF
172 applicator. The RF power was set automatically by controlling the voltage to the power
173 amplifier from the generator, which was fed in the middle of upper electrode back side and
174 proportional to the electrode gap by changing the top electrode position with the aid of
175 adjustable screws (Fig. 2). A 1-cm-thick polystyrene sheet with the area of $83 \times 40 \text{ cm}^2$ (same
176 as the top electrode) was placed above the bottom electrode to prevent direct contact between
177 the electrode and the container. The polystyrene container with a bottom thickness of 2 cm
178 was placed in the center of the polystyrene sheet for achieving better RF heating uniformity

179 (Huang et al., 2015c; Tiwari et al., 2011a; Jiao et al., 2015a). To ensure repeatability of the
 180 experimental results and limit the influence of non-uniform electromagnetic fields on sample,
 181 the location of the sample was fixed on the center and middle between the top and bottom
 182 electrodes during all experiments (Llave et al., 2015).



183

184

Fig. 2. Schematic diagram of the 6 kW, 27.12 MHz RF system.

185 2.4.2. Governing equations

186 The electric field distribution within the load (food sample and the container) and at any
 187 point inside the electrodes were given by the solution of the Gauss law derived from a
 188 quasi-static approximation of Maxwell's equations (Marra et al., 2007):

$$189 \quad \nabla(\varepsilon \cdot \vec{E}) = 0 \quad (1)$$

190 where ε is permittivity of the load and \vec{E} is the electric field vector. Simulation of RF heating
 191 as a quasi-static electric field between the electrodes was preferred since the wavelength (11
 192 m) in the 27.12 MHz RF system is often much larger than the analyzed domain sizes.

193 The RF power conversion to thermal energy (Q , $W\ m^{-3}$) within the food sample under an
 194 electric field intensity ($|\vec{E}|$, $V\ m^{-1}$) are described as follows (Choi & Konrad, 1991):

$$195 \quad Q = 2\pi f \varepsilon_0 \varepsilon'' |\vec{E}|^2 \quad (2)$$

196 where f is the frequency (Hz), ε_0 is the permittivity of electromagnetic wave in free space
 197 ($8.86 \times 10^{-12}\ F\ m^{-1}$), ε'' is the relative dielectric loss factor of the sample load, and $|\vec{E}|$ is the
 198 modulus of the $E(x, y, z)$ field.

199 Evaluating the absorbed RF power density at any point inside the sample requires the
 200 value of \vec{E} , which is a function of the sample geometry and DPs as well as the electrode
 201 configuration (Jiao et al., 2014b; Marshall & Metaxas, 1998):

$$202 \quad |\vec{E}| = \frac{V}{\sqrt{(\varepsilon' d_{air} + d_{mat})^2 + (\varepsilon'' d_{air})^2}} \quad (3)$$

203 where d_{air} is the air gap between top electrode and food sample (m), d_{mat} is the height of the
 204 food material (m), and V is the voltage between the two electrodes (V).

205 The heat equation was solved within the food material and the container, considering the
 206 internal conduction and the heat generation due to RF energy, while external convection at the
 207 sample surface was taken into account in the boundary conditions. Therefore, the temperature
 208 distribution was simulated based on a 3D heat transfer equation, including solution of Fourier
 209 heat transfer equation plus a generation term, coupled with the quasi-static electro-magnetic
 210 field equations (Uyar et al., 2015):

$$211 \quad \rho C_p \frac{\partial T}{\partial t} = \vec{\nabla} \cdot k \vec{\nabla} T + Q \quad (4)$$

212 where ρ is density ($kg\ m^{-3}$), C_p is specific heat ($J\ kg^{-1}\ K^{-1}$), k is thermal conductivity ($W\ m^{-1}$
 213 K^{-1}), T is the temperature (K), and t is the time (s). While the solution of heat transfer is

214 needed just within the sample, the Gauss law must be evaluated for the space between the two
215 electrodes, which includes the sample and the air around it (Marra et al., 2007).

216 2.4.3. Geometric model

217 The 3D geometric model was developed using COMSOL (V4.3a COMSOL Multiphysics,
218 COMSOL, Co., LTD., Shanghai, China) based on the actual structure and size of the 6 kW,
219 27.12 MHz RF system (Fig. 3). The complete geometric model included RF cavity (129×109
220 $\times 52 \text{ cm}^3$), top ($83 \times 40 \text{ cm}^2$) and bottom electrode ($99 \times 59 \text{ cm}^3$), polystyrene sheet (83×40
221 $\times 1 \text{ cm}^3$), soybean flour sample ($30 \times 22 \times 6 \text{ cm}^3$), and polystyrene container ($34 \times 26 \times 8 \text{ cm}^3$)
222 as shown in Fig. 3. Soybean flour samples were placed in the center and middle between the
223 top and bottom electrodes with an air gap of 3 cm. The whole domain in this study was
224 divided into three sub-domains, the food sample (SD1), container (SD2), and the surrounding
225 air (SD3). In SD1 and SD2, both heat transfer and Gauss law equations were solved, whereas
226 in SD3 only dielectric phenomenon was considered. An unstructured mesh consisting of
227 Lagrange quadratic elements was created over the entire domain of RF cavity. The extremely
228 fine mesh structure was preferred based on the convergence tests even though it led to longer
229 computational times, which consisting of 122,868 domain elements (tetrahedrons), 10,574
230 boundary elements (triangles) and 879 edge elements (linear). The top electrode was drawn as
231 an embedded element (work plane) in 3D to avoid a large number of mesh elements for a thin
232 electrode plate. The X , Y , and Z directions were modeled using a mesh spacing of 5 mm,
233 which provided satisfactory spatial resolution for the considered domain and the solution was
234 found to be independent to the grid size with further refinement.

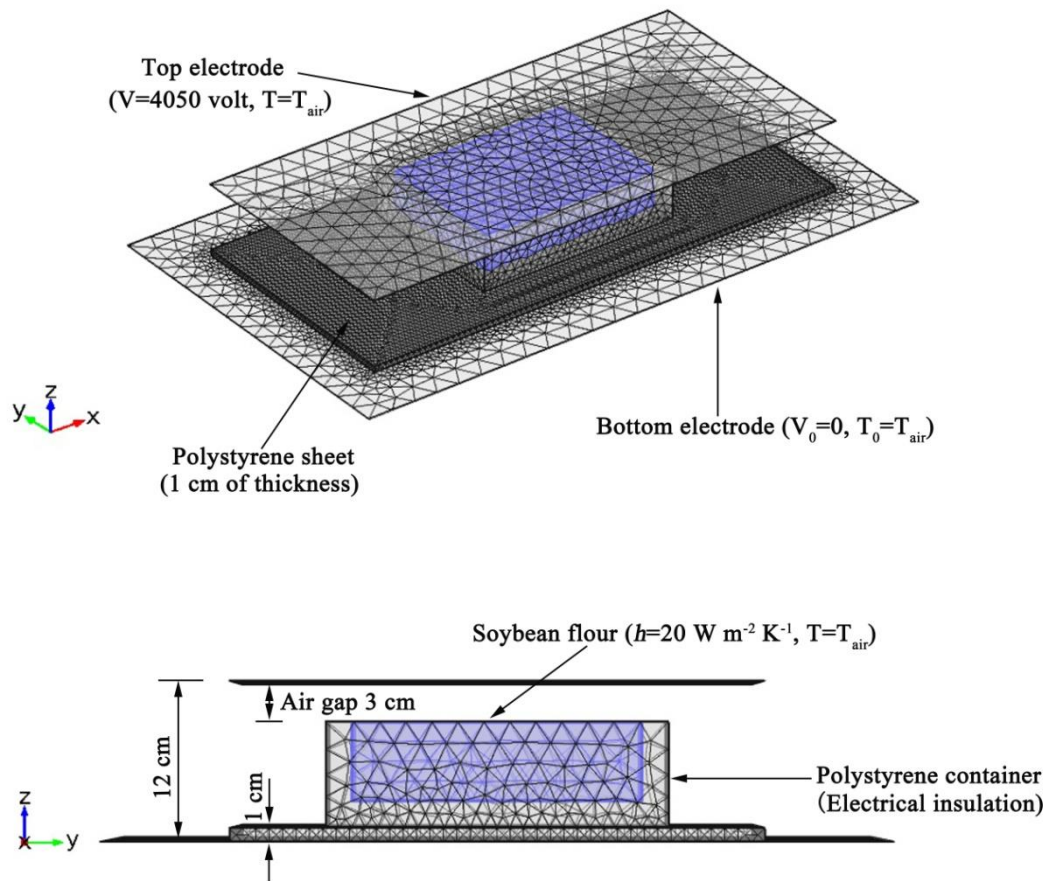


Fig. 3. 3D model approach of RF heating system (mesh of 5 mm).

2.4.4. Thermo-physical and dielectric properties

The moisture content of soybean flour was determined by drying triplicate 3-5 g flour samples in aluminum moisture dishes in an oven (DZX-6020B, Shanghai Nanrong Co. Ltd., Shanghai, China) at 130 °C for 1 h until a substantially constant weight was obtained (AOAC, 2002). The density of soybean flour was calculated from the measured mass and volume at room temperature over three replicates. The specific heat and thermal conductivity of soybean flour were measured using a differential scanning calorimeter (DSC, Q2000, TA Instruments, New Castle, PA, USA). An empty sealed aluminium pan was used as a reference and 10 mg soybean flour samples were sealed in another aluminium pan (20 µL). The procedure included cooling the sample from room temperature to 0 °C, equilibrating for 6 min, and then heated in the DSC at a rate of 10 °C/min over a temperature range of 20-80 °C. Each measurement was repeated three times and details of the measurement system and procedure can be found

249 elsewhere (Jiao et al., 2014b). These data were subjected to linear regression analysis for
 250 using these properties in simulation model over the treatment temperatures range from 20 to
 251 60 °C (suitable for postharvest pest control). Dielectric properties of the soybean flour sample
 252 had a non-linear relationship with temperature and were reported at frequencies of 27 MHz
 253 (Guo, Wang, Tiwari, Johnson, & Tang, 2010). Dielectric and thermo-physical properties of
 254 the electrode and ambient air at room temperature (20 °C) were adapted from COMSOL
 255 material library (Table 2).

256 Table 2. Electrical and thermo-physical properties of materials used in computer simulation.

Property	Electrode ^a	Air ^a	Polystyrene ^b	Soybean flour
Density (ρ , kg m ⁻³)	2700	1.2	25	380
Specific heat (C_p , J kg ⁻¹ K ⁻¹)	900	1000	1300	$5.8 \cdot T + 1614$
Thermal conductivity (k , W m ⁻¹ K ⁻¹)	160	0.026	0.036	$0.0007 \cdot T + 0.083$
Dielectric constant (ϵ')	1	1	2.6	3.96^c
Loss factor (ϵ'')	0	0	0.0003	0.38^c

257 Source: T = temperature (°C)

258 ^a COMSOL material library, V4.2a (2012).

259 ^b Huang et al. (2016).

260 ^c Guo et al. (2010).

261 2.4.5. Initial and boundary conditions

262 The Gauss law needs boundary conditions for the electrodes and the RF cavity walls to
 263 determine the electric field distribution inside the system.

264 – Top electrode was set as the electromagnetic source since it introduced high frequency
 265 electromagnetic energy from the generator to the heating cavity, which maintained at a certain
 266 potential V and constant during the processing time.

267 – All the metal shielding parts except for the top electrode were maintained at the ground
268 condition ($V_0 = 0$).

269 – The metallic RF cavity walls and the plastic container were assumed to be electrically
270 insulated ($\nabla \cdot \vec{E} = 0$), and for the left and right sides of the system, the surrounding air was
271 considered.

272 For the heat transfer equation to determine the temperature distribution inside the system:

273 – The initial temperature of the two electrodes, surrounding air, polystyrene sheet, and
274 polystyrene container was set at room temperature (20 °C), and the initial temperature of the
275 soybean flour was assumed at a uniform temperature ($T_0 = 20$ °C).

276 – The inlet and outlet of the simulated system were adjusted to meet the condition $T = T_a$,
277 where T_a is the ambient temperature, the top and bottom sides (the external sides of the upper
278 and lower electrodes) were thermally insulated ($\nabla T = 0$).

279 – The load was considered to be subjected to heat exchange with surrounding air by
280 convection expressed as:

$$281 \quad -k \frac{\partial T}{\partial n} = h(T - T_a) \quad (5)$$

282 Heat exchange was approximated by assuming a convective heat transfer coefficient ($h =$
283 $20 \text{ W m}^{-2} \text{ K}^{-1}$, which is a typical value used for natural convection in air in the used
284 configuration), T_a is the air temperature inside the RF cavity (20 °C) and \hat{n} is the normal
285 vector.

286 2.3.6. Constant electric potential

287 Even though the voltage varies all over the surface of the top electrode, it was assumed to
288 be uniform since the electrode dimensions ($0.83 \times 0.4 \text{ m}^2$) were much lower than 30% of the
289 RF wave length ($\approx 11 \text{ m}$). Thus, the calculation with constant electric potential applied at the

290 top electrode was performed by the following equation with the measured anode current (I_a)
291 (Zhu, Huang, & Wang, 2014):

$$292 \quad V = 11242I_a + 2029.9 \quad (6)$$

293 On the basis of the measured anode current (0.18 A), the top electric voltage applied was
294 set at 4050 V for subsequent simulations. Based on our preliminary results, the voltage V
295 varies up to 11% between standby and full-load conditions while Marshall and Metaxas (1998)
296 reported that the difference was only 7%. Llave et al. (2015) also reported the similar heating
297 problems associated with the free-running oscillator systems.

298 2.3.7. Model assumptions

299 In the current simulation study, the following assumptions were considered to simulate
300 temperature distribution of soybean flour subjected to RF heating:

301 – DPs and TPs (thermo-physical properties) of soybean flour were assumed to be
302 homogeneous and isotropic, the density and dielectric properties were assumed temperature
303 independence.

304 – The mass and momentum transfers of water were ignored due to a short RF heating
305 time (5 min) and the influence on moisture content was unnoticeable (< 2%) based on
306 preliminary study.

307 2.3.8. Solution methodology

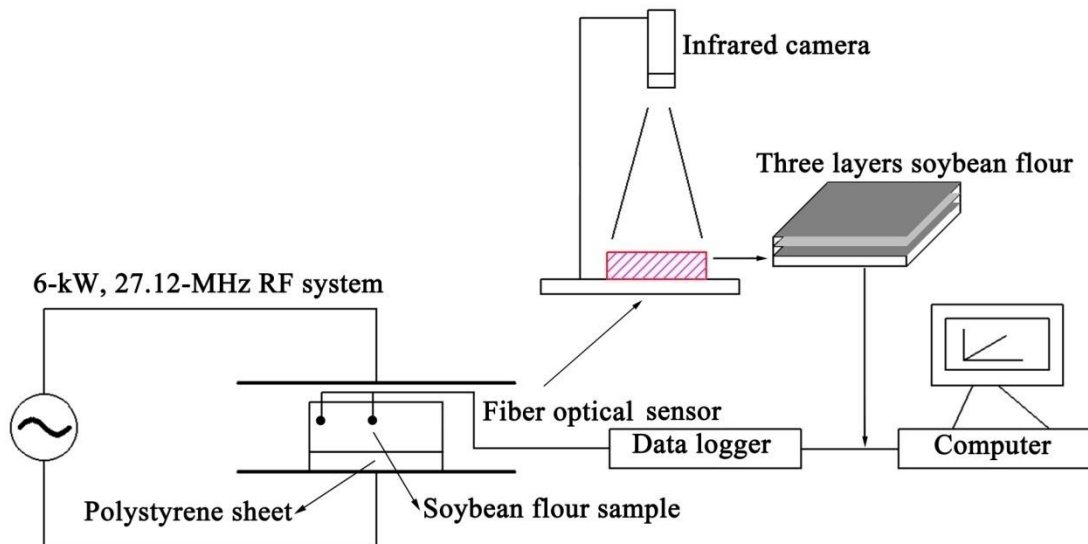
308 The Joule heating module of a finite element based software COMSOL was used to solve
309 this multi-physics problem that involves the solution of electromagnetic equation coupled
310 with heat transfer equation. The important stages of the computer simulation included
311 defining transport equations or domain and sub-domains of interest, describing dielectric and
312 thermo-physical properties, setting up boundary conditions, meshing of the domains, and
313 choosing the final numerical solver. All computer simulations were performed on a Dell
314 workstation with an Intel® Core™ i5-2400, 3.10-GHz processor and 8 GB RAM running a

315 Windows 8.1 64-bit operating system. The maximum and minimum mesh element sizes were
316 0.0578 m and 0.000578 m, respectively. Time step was determined by the max iteration per
317 time step. If the computations were convergent before the max iteration, the time step could
318 be short and would start next iteration automatically. Based on extensive testing, the
319 maximum iteration per time step was 10^4 , and initial and maximum time steps were set as
320 0.001 and 1 s, respectively. The direct linear system solver UMFPACK was used for all
321 calculations with a relative tolerance and an absolute tolerance of 0.01 and 0.001.
322 Simultaneous solution of the coupled transient equations took nearly 5400 s (1.5 h) for
323 simulating 300 s of RF heating process at 1-s intervals.

324 2.4. RF experiments

325 In experiments, soybean flour samples with density of 380 kg m^{-3} were put into the
326 rectangular container and positioned coaxially in the center and middle between the top and
327 bottom electrodes of the RF system. The lethal temperature range for the complete mortality
328 of many insects including *Indianmeal moth* at all life stages was within $44\text{-}52^\circ\text{C}$ with
329 different holding time (Johnson, Wang, & Tang, 2003). To meet the required insect mortality
330 and acceptable product quality, the soybean flour samples were subjected to RF heating for 5
331 min with electrode gap of 12 cm according to our previously published RF power
332 recommendations (Huang et al., 2015c). Sample temperature-time histories at two
333 representative locations in middle layer of soybean flour were measured using a six-channel
334 fiber optical temperature measurement system with an accuracy of $\pm 1^\circ\text{C}$. Probes connected
335 with two channels were inserted into the center and corner of soybean flour through predrilled
336 holes while the remaining channels were used to monitor the air temperature inside the RF
337 cavity (Fig. 1). Temperatures were sampled every second and recorded at 1-s intervals over 5
338 min. After 5 min RF heating, the container was immediately taken out from the RF cavity,
339 and the surface temperature of soybean flour from top to bottom layer was measured by an

340 infrared camera. All three thermal imaging recordings were completed in 20 s. The image
341 analysis system (V1.0, DaLi Science and Technology Co., LTD, Zhejiang, China) was used to
342 collect and analyze the surface temperature data of soybean flour, and 97,856 individual
343 temperature data were collected in each layer. The whole experiments were replicated five
344 times and the experimental setup for sample temperature measurements during RF heating are
345 shown in Fig. 4. The measured temperature profiles and the isothermal curves of soybean
346 flour were used to validate the developed simulation model. Average and standard deviation
347 values in the temperature of the RF heated samples were also compared over three layers.



348

349 Fig. 4. Experimental setup for sample temperature measurements in RF heating.

350 2.5. Statistical analysis

351 Means and standard deviations were calculated with Sigma-Plot 12.0 (Systat Software,
352 Inc., San Jose, CA, USA) statistical software. Sigma-Plot was used to perform t-test, one way
353 analysis of variance (ANOVA) and Least Significant Difference test (LSD) at a 95%
354 confidence level ($P < 0.05$) to identify difference among samples. To validate the simulation
355 results, the root mean square error (RMSE) was calculated for the comparison of temperature
356 differences between the simulated and experimental profiles over N time steps.

$$RMSE = \sqrt{\frac{1}{N} \sum_{i=1}^N \left[\frac{T_{exp}(i) - T_{sim}(i)}{T_{exp}(i)} \right]^2} \quad (7)$$

where T_{exp} and T_{sim} are the experimental and simulated temperature ($^{\circ}\text{C}$), respectively, i is the data node number, and N is the total number of points.

2.6. Heating uniformity evaluation

Cold spot locations were determined by finding the lowest temperature from thermal images and simulated temperature profiles, which were located at the center part of each layer (Huang, Chen, & Wang, 2015a). In this study, all simulations were conducted based on the top surface center (cold spot) to reach the target disinfestation temperature (50°C) after 5 min RF heating. The relative sensitivity with respect to model inputs was evaluated using the temperature uniformity index (UI) inside the samples under the same electrode gap of 12 cm. It would reflect the degree to which temperature in the volume deviated from the target temperature (Jiao et al., 2015b):

$$UI = \frac{\int_{V_{vol}} \sqrt{(T - T_t)^2} dV_{vol}}{(T_t - T_{initial})V_{vol}} \quad (8)$$

where T_t and $T_{initial}$ are the target and initial temperatures ($^{\circ}\text{C}$) inside the dielectric material over the volume (V_{vol} , m^3). A smaller index corresponds to a better heating uniformity.

372

2.7. Simulation sequence

2.7.1. Simulation with varying DPs of the sample and container

The RF heating uniformity was significantly influenced by DPs of the treated material. After the model has been validated by comparing its results with the experimental ones, to study the effect of container dielectric constant on UI of the sample, simulations were run by changing dielectric constant of the container from 0.1 to 19, with various sample dielectric constants ranging between 2 and 13. Electrode gap in each simulation was set at 12 cm with

380 heating time of 5 min. The top electrode voltage was determined by running multiple
381 simulations with different input voltage values until the lowest temperature at the top surface
382 center (cold spot) to reach 50 °C (Jiao et al., 2015b). Another set of simulations were
383 performed with container loss factor varied between 0.00003 and 0.3 and sample loss factor
384 increased from 0.1 to 5 to study the effect of container loss factor on UI. Regression equations
385 could be established for the DPs of the sample and container based on the minimum UI
386 values.

387 2.7.2. Simulation with varying density of sample and container

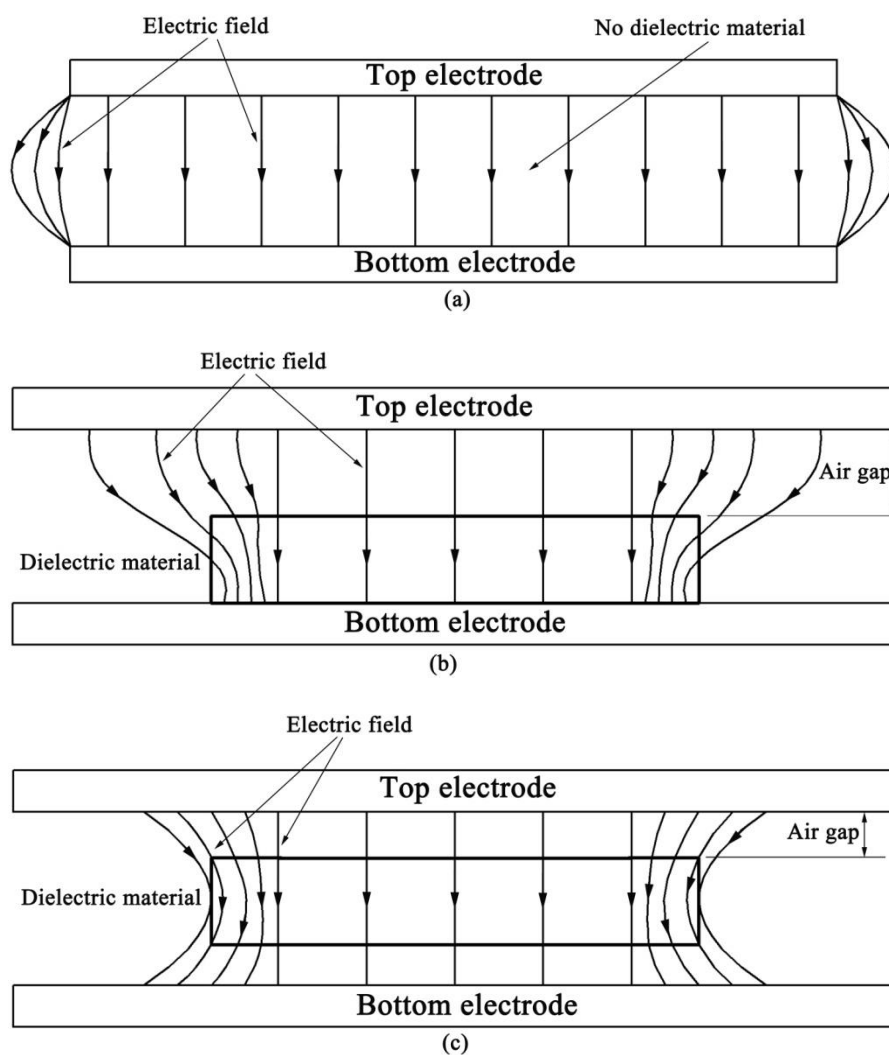
388 Since the specific heat and thermal conductivity had a relatively slight effect on RF
389 heating uniformity based on previous studies (Huang, Zhu, & Wang, 2015b; Tiwari et al.,
390 2011b), a series of simulations were run by changing container density progressively between
391 20 and 1000 kg m⁻³, while the density of the processed food was fixed as 300, 500, 800, and
392 1000 kg m⁻³, respectively. Trends of the UI of soybean flour in each simulation were
393 determined and the container density values corresponding to the minimum UI could be
394 calculated using Matlab 2010 (Mathworks Inc., Natick, MA). Therefore, the density
395 correlations between the surrounding container and treated products could be developed.

396 **3. Results and discussions**

397 3.1. Simulated electric field distribution for soybean flour

398 Figs. 5a-c show the general trends of electric field distributions between two parallel
399 plate electrodes without dielectric material, and with dielectric material placed on the bottom
400 and middle between two electrodes. The electric field between two parallel plate electrodes
401 was in parallel lines uniformly spaced throughout the region between two electrodes, and
402 perpendicular to their surfaces with no dielectric material placed in it (Fig. 5a). When the
403 dielectric material was placed at the center of the bottom electrode with an air gap over it, the
404 presence of the surrounding air causes an intensification of the heating near the top of the

405 electrode space at the edges of the material (Fig. 5b). As observed in Fig. 5c, the electric field
 406 was distorted in the presence of the dielectric material placed in the middle of two parallel
 407 plate electrodes. Samples placed in the middle of RF electrodes showed higher electric field
 408 intensity at their central section as electric field deflected by both (top and bottom) edges with
 409 increased net electric field concentration at the central parts of the sample (Tiwari et al.,
 410 2011a). This demonstrated the significant effect of surrounding material (usually air) on
 411 obtaining uniform electric field distributions inside the product.



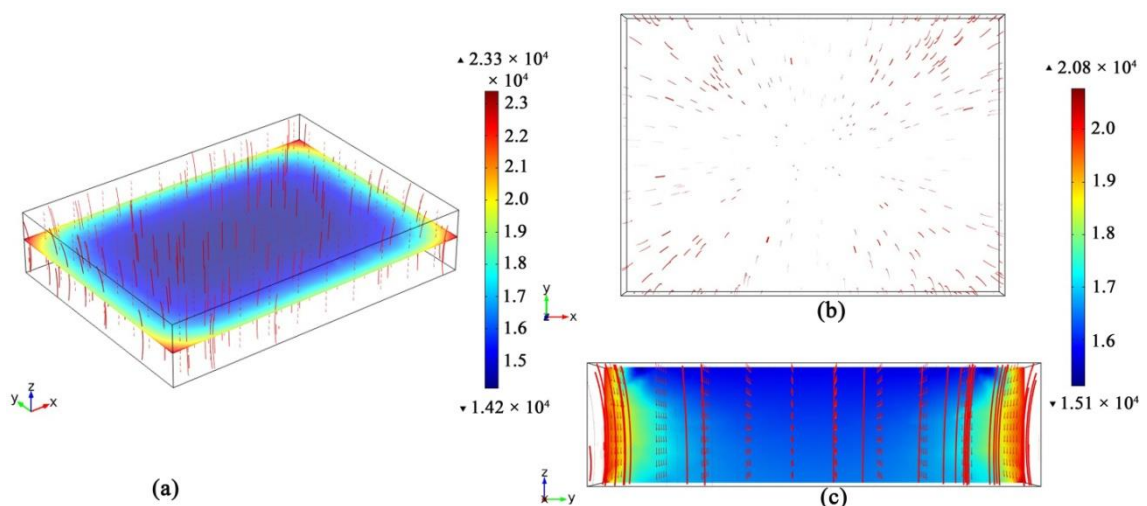
412 (a)

413 (b)

414 (c)

415 Fig. 5. The electric field strength between two parallel plate electrodes with (a) no dielectric
 416 sample, (b) dielectric sample placed on the center of bottom electrode, (c) and dielectric
 417 sample placed in the center and middle between top and bottom electrodes with a fixed
 418 electrode gap of 12 cm and initial temperature of 20 °C.

419 Figs. 6a-c show the simulated spatial E-field distributions of soybean flour in the middle
 420 layer of whole sample ($z = 4$ cm), top horizontal layer ($z = 6$ cm) and vertical ($x = 11$ cm)
 421 cross section after 5 min RF heating at a fixed electrode gap of 12 cm. In the whole 3-D
 422 model of the rectangular shaped sample, high electric field concentrations occurred at the
 423 corners and edges due to the refraction and reflection of the electrical field at these parts (Fig.
 424 6b). Horizontally, electric field lines all bending at the interfaces between soybean flour and
 425 the contacted container side walls (Fig. 6a). As a result, net electric field increased at four
 426 sides and edges of the treated sample. In the vertical center cross section ($x = 11$ cm), the
 427 electric field distribution was more uniform in the top and bottom than other sections but
 428 concentrated at the side walls and center parts of the sample (Fig. 6c). The merging of two or
 429 more electric field lines at the edges and corners resulted in a higher volumetric power density,
 430 hence, overheating occurred in these areas more than on the flat surfaces (Fu, 2004). The
 431 electric intensification was greater for samples either having a higher or lower dielectric
 432 constant than for those surrounding materials (Huang et al., 2015c; Tiwari et al., 2011a).
 433 Therefore, it is necessary to devise means to eliminate the electromagnetic field concentration
 434 phenomenon within the treated products.



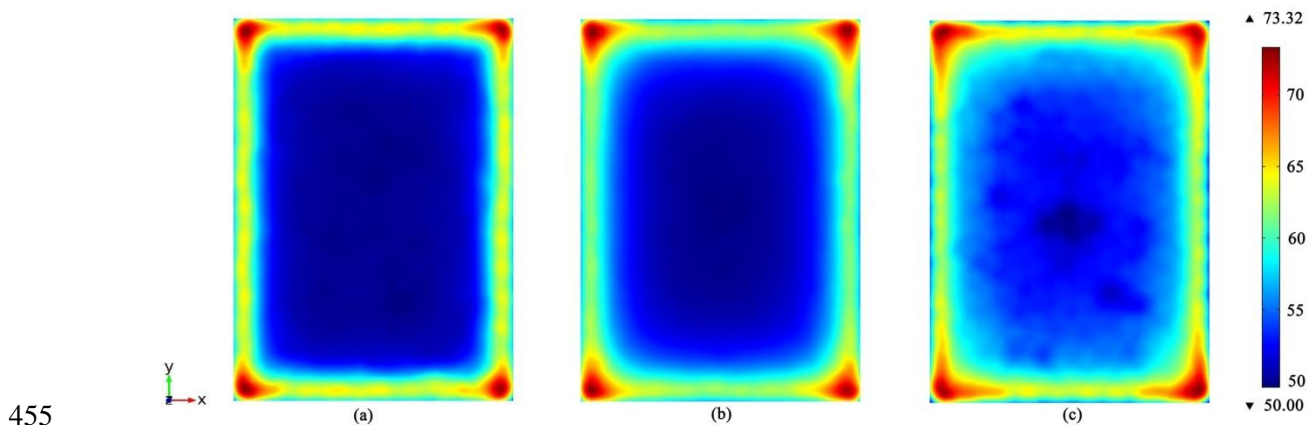
435 (a)
 436 Fig. 6. Simulated electric field direction (arrow), electric field intensity (color surface, $V\ m^{-1}$),
 437 and electric potential (streamline) of soybean flour ($30 \times 22 \times 6\ cm^3$) in (a) middle layer of

438 whole sample ($z = 4$ cm), (b) top horizontal layer ($z = 6$ cm), and (c) vertical ($x = 11$ cm)
439 center cross sections after 5 min RF heating with an electrode gap of 12 cm and initial
440 temperature of 20 °C.

441

442 3.2. Simulated temperature profiles for soybean flour

443 The results presented in Fig. 6 showed that corners, edges, and middle parts had higher
444 electric field concentration when the sample was placed in the center and middle between the
445 top and bottom electrodes. Figs. 7a-c corroborate the result as the maximum temperature
446 values appeared at the corners and edges of all layers. In three horizontal layers, the
447 temperature values were higher in the middle layer (51-74°C), whereas they were lower in the
448 top and bottom layers (50-69°C and 52-67°C). The highest temperature values occurred at the
449 center parts of soybean flour over the volume, placed in the middle (3 cm above the bottom
450 electrode) between two RF electrodes (Fig. 3). The non-uniform temperature distribution
451 could be attributed to the electric field behaviour, which was deflected at the sample corners
452 and edges, resulting in higher temperature values at these parts (Fig. 7). These findings are
453 corroborated by overheating at edges and center parts of the fish (Llave et al., 2015), raisins
454 (Alfaifi et al., 2014), and wheat kernels (Jiao et al., 2015a) subjected to RF treatment.



456 Fig. 7. Simulated temperature distributions (°C) at (a) top ($z = 2$ cm), (b) middle ($z = 4$ cm),
457 and (c) bottom ($z = 6$ cm) layers of soybean flour ($30 \times 22 \times 6$ cm³) placed in the center and

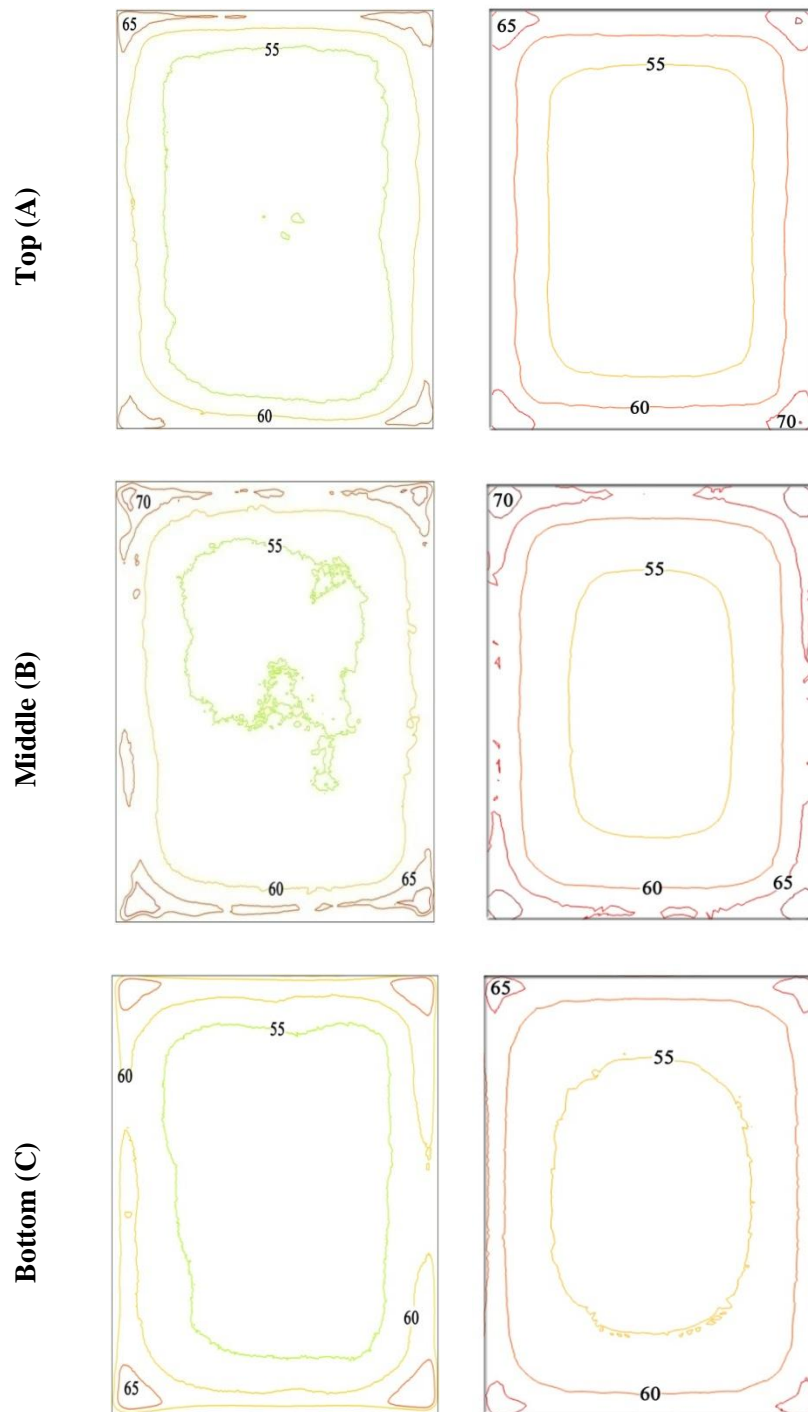
458 middle between two electrodes after 5 min RF heating at an electrode gap of 12 cm and initial
459 temperature of 20 °C.

460 3.3. Computer model validation

461 The simulated spatial temperature profiles of soybean flour over three layers were
462 compared with the experimental results obtained using a thermal imaging camera (Fig. 8).
463 Both results demonstrated that the experimental temperature distribution showed good
464 agreements with the simulated data in center parts of the top, middle, and bottom layers. For
465 corners and edges of the sample, the maximum temperature differences in top, middle, and
466 bottom layers were about 4, 5, and 3 °C, respectively. The temperature differences between
467 experiment and simulation might be caused by the simplification of the RF units or ignored
468 moisture and heat loss in the possible evaporation in the soybean flour samples. Fig. 9 shows
469 the measured and simulated time-temperature profiles of soybean flour at center and corner
470 positions (as demonstrated in Fig. 1). Both sets of data exhibited similar trends, with the
471 heating rate of 5.2 °C/min for corner and 4.8 °C/min for center throughout the duration of the
472 heating process. Acceptable RMSE values were obtained for corner (0.014 °C) and center
473 (0.017 °C), respectively. Table 3 compares simulated and experimental average and standard
474 deviation temperatures of all three layers after 5 min RF heating. Five replicates of
475 experimental average temperatures were slightly lower than simulated ones, which were
476 attributed to the heat loss when samples were transferred from the RF cavity to the camera.
477 The simulated standard deviations were comparatively higher than those determined by
478 experiments. This was probably caused by more data points for corners with fined meshes in
479 simulation, while these were equally distributed in experiment. It was corroborated that the
480 simulated temperature profile in all three layers could capture the actual temperature field
481 variation, and the model accuracy could be guaranteed.

Experimental

Simulated



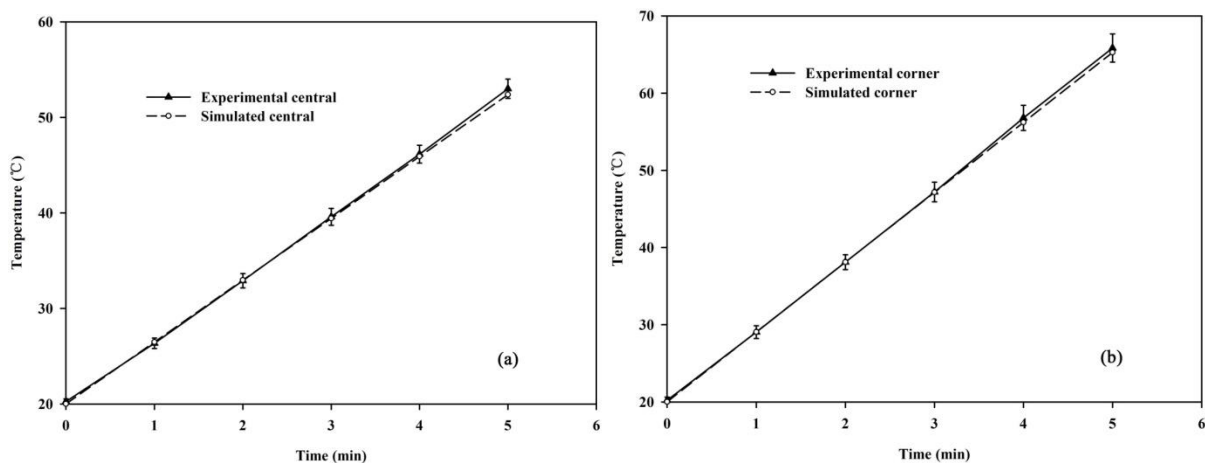
482 Fig. 8. Comparison of simulated and experimental temperature distributions in top (A),
 483 middle (B), and bottom layers (C) of soybean flour placed in a polystyrene container (30×22
 484 $\times 6 \text{ cm}^3$) in the center and middle between the top and bottom electrodes after 5 min RF
 485 heating at a fixed electrode gap of 12 cm and initial temperature $20 \text{ }^\circ\text{C}$.

486

487 Table 3. Comparison between simulated and experimental temperatures (Ave \pm SD, $^{\circ}$ C) in
 488 three different horizontal layers of soybean flour placed in the center and middle between two
 489 electrodes after 5 min RF heating with an electrode gap of 12 cm and initial temperature of
 490 20 $^{\circ}$ C.

Layer	Simulated ($^{\circ}$ C)	Experimental ($^{\circ}$ C)
	Ave \pm SD	Ave \pm SD
Upper	57.9 \pm 4.4	56.8 \pm 3.9
Middle	59.6 \pm 5.4	58.8 \pm 4.1
Bottom	56.8 \pm 3.8	56.1 \pm 3.2

491



492

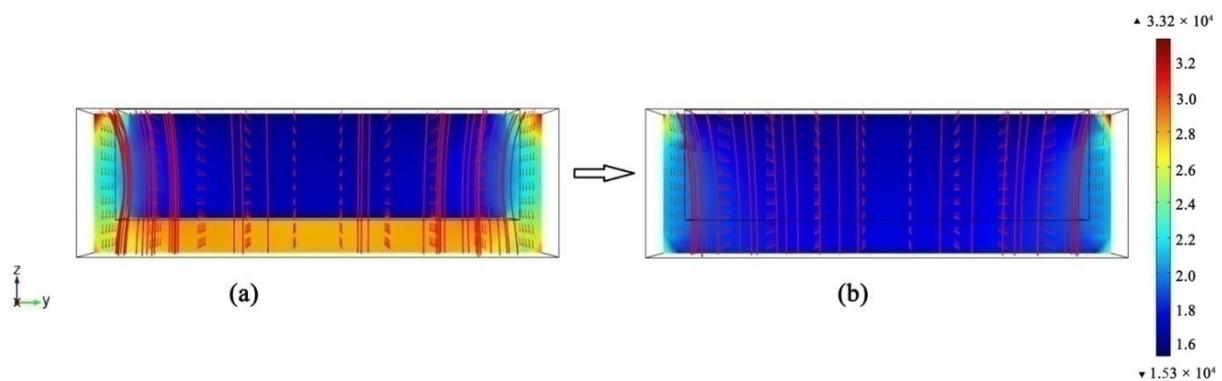
493 Fig. 9. Experimental and simulated temperature-time histories of soybean flour at the center (a)
 494 and corner (b) positions of middle layer ($z = 4$ cm), placed in a polystyrene container in the
 495 center and middle between the top and bottom electrodes during 5 min heating at a fixed
 496 electrode gap of 12 cm (bars indicate standard deviation of five runs).

497

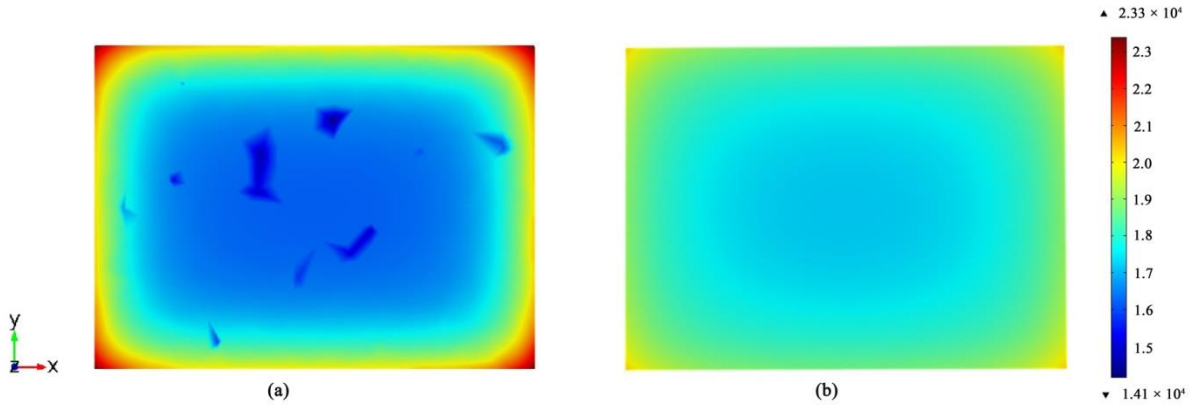
498 3.4. Effect of DPs of sample and container on sample temperature distribution

499 Fig. 10 shows the electric field intensities in polystyrene container and soybean flour
 500 samples with container dielectric constant of 2.6 and 3.96, respectively. Simulated results

501 illustrated how electric field patterns were distorted within the rectangular shaped sample, and
502 severe edge heating usually happened at four corners and the bottom sections of sample-wall
503 interfaces. When the dielectric constant differences between surrounding material and treated
504 sample was greater, deflection and distortion of the electric field increased more frequently at
505 the contact surface of two different materials (Fig. 10a). The electric field distortion was
506 reduced when the container dielectric constant changed to 3.96 (equal to the treated sample).
507 The maximum electric field intensity decreased from $3.32 \times 10^4 \text{ V m}^{-1}$ over the whole
508 treated sample and surrounding container (Fig. 10b). The top electrode voltage used in
509 computer simulation was 4200 V determined by running multiple simulations with different
510 inputted voltages until the target temperature ($50 \text{ }^\circ\text{C}$) was obtained at the top surface center
511 (cold spot) of soybean flour (Jiao et al., 2015b). The electric field distortion was reduced with
512 the maximum electric field difference of middle layer reduced from 0.92 to $0.51 \times 10^4 \text{ V m}^{-1}$
513 after changing dielectric constant of the surrounding container (Fig. 11). The standard
514 deviation of temperature and electric field at three horizontal layers of soybean flour was also
515 reduced as shown in Table 4. Simulated UI of soybean flour decreased from 0.112 to 0.083
516 over the volume, demonstrating a rather uniform temperature obtained after 5 min RF heating.
517 Therefore, different electric field patterns between surrounding container and food products
518 could be minimized by appropriately matching DPs of the container with that of treated
519 material.



521 Fig. 10. Simulated electric field direction (arrow), electric field intensity (color surface, V
 522 m^{-1}), and electric potential (streamline) of soybean flour and polystyrene container with
 523 container DPs of (a) $2.6-j*0.0003$ and (b) $3.96-j*0.0003$ after 5 min RF heating under the
 524 fixed sample DPs of $3.96-j*0.38$.



525
 526 Fig. 11. Simulated electric field distribution (V m^{-1}) of soybean flour in the middle layer with
 527 container DPs of (a) $2.6-j*0.0003$ and (b) $3.96-j*0.0003$ after 5 min RF heating under the
 528 fixed sample DPs of $3.96-j*0.38$.

529

530 Table 4. Simulated temperature (Ave \pm SD, $^{\circ}\text{C}$) and electric field intensity (Ave \pm SD, V m^{-1})
 531 of soybean flour in three different layers with container DPs of $2.6-0.0003\cdot j$ and $3.96-0.0003\cdot j$
 532 under the fixed electrode gap of 12 cm.

Container	$2.6-0.0003\cdot j$		$3.96-0.0003\cdot j$	
DPs				
Layer	Temperature ($^{\circ}\text{C}$)	Electric field (V m^{-1})	Temperature ($^{\circ}\text{C}$)	Electric field (V m^{-1})
Upper	57.9 ± 4.4	18886.2 ± 1488.4	59.3 ± 3.1	19329.6 ± 923.3
Middle	59.6 ± 5.4	19063.3 ± 1957.5	61.8 ± 4.3	20125.4 ± 1226.5
Bottom	56.8 ± 3.8	17151.9 ± 1019.7	58.1 ± 2.1	18255.1 ± 864.4

533

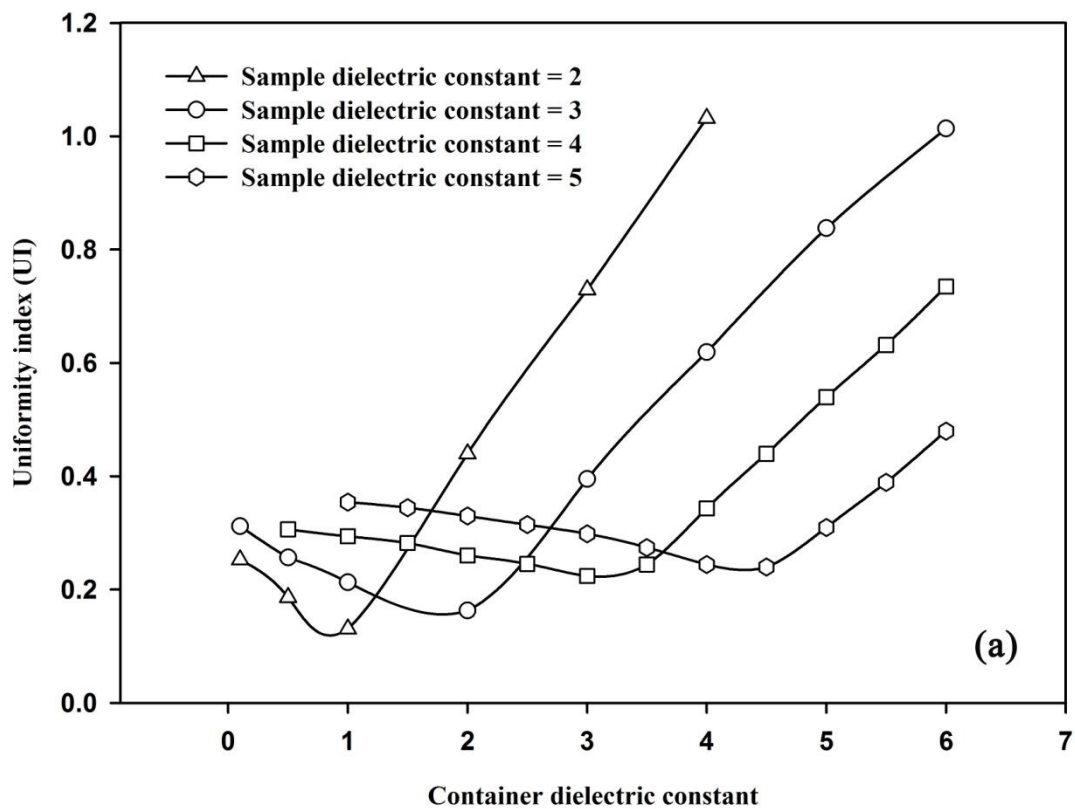
534 3.5. Effect of DPs of sample and container on sample UI

535 Figs. 12a-c summarize the results of a series of simulations with surrounding container
536 dielectric constant ranging from 0.1 to 19, and sample dielectric constants increasing
537 progressively at regular intervals between 2 to 13, based on the previous measured DPs of
538 soybean flour (Guo et al., 2010). Simulated results demonstrated that increase in container
539 dielectric constant caused initial reduction and then the increase of UI with the fixed sample
540 dielectric constant values. UI was the lowest when the surrounding container dielectric
541 constant was smaller than the sample's one if dielectric constant of heated sample was < 7 .
542 But for the dielectric constant of heated sample ≥ 7 , UI started to get the minimal value when
543 the surrounding container dielectric constant was greater than the sample's one. It was
544 interesting to notice that UIs had their minimum values whenever the dielectric constants of
545 surrounding container were in a comparable range with the sample's one. This was contrary to
546 a general concept that increasing dielectric constant of the surrounding container for equal to
547 the sample's one might obtain the best heating uniformity of the heated products. Logistic
548 regression analysis was performed to determine the minimum values of UI by solving a set of
549 quadratic equations based on the simulated trends of UI as illustrated in Fig. 12. Therefore,
550 dielectric constants of the surrounding container could be determined by solving the roots of
551 the regression equations. Table 5 shows the calculated dielectric constants of the surrounding
552 container when the UI achieved the lowest values with various sample dielectric constants.
553 The simulated voltages used in the computer simulation were in a range of 2860-9300 V in
554 order to make the lowest temperature reach 50 °C. It is clear that trends of simulation voltage
555 change depended on the dielectric constant of sample and the surrounding container. Since the
556 voltage level along the upper electrode is proportional to the square of dielectric constant of
557 treated sample, it also increased with the increase in dielectric constant (Birla, Wang, & Tang,
558 2008).

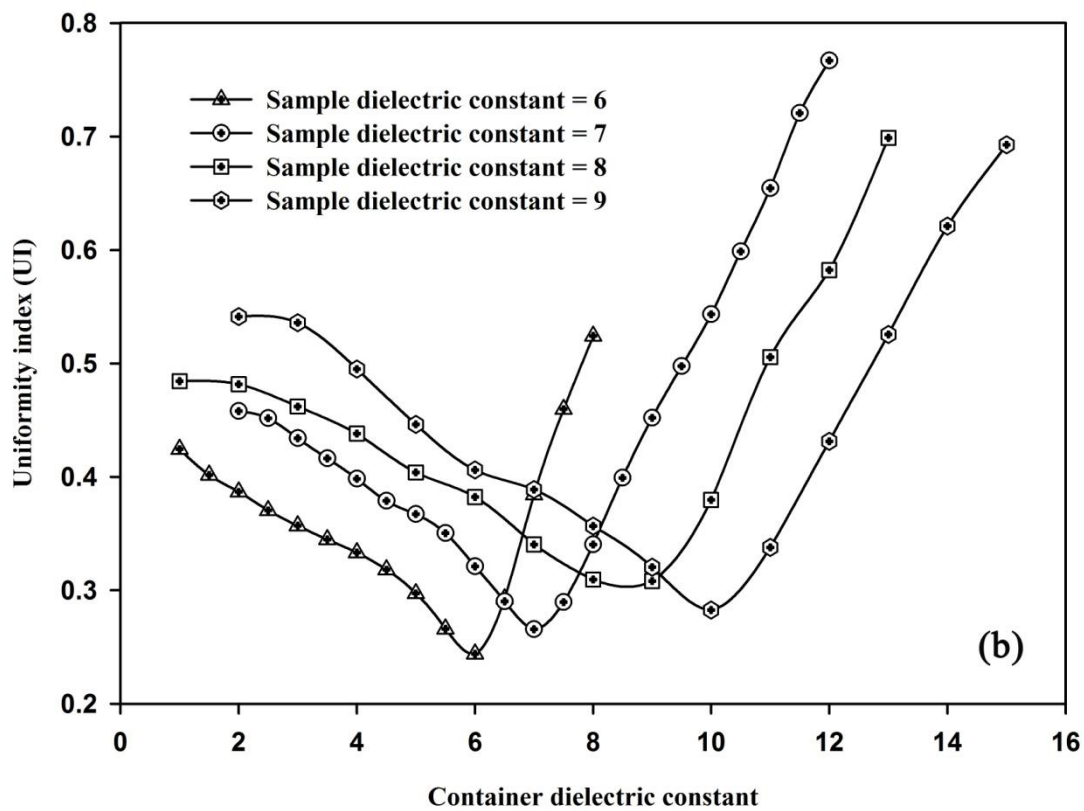
559 Fig. 13 shows the general trends of dielectric constant correlations between surrounding
560 container and treated soybean flour for ensuring good RF heating uniformity. It is clear that
561 dielectric constant of surrounding container increased almost linearly with increasing
562 dielectric constant of heated sample. The dielectric constant of surrounding container as a
563 function of sample's one may be predicted according to the following regression equation
564 with a high coefficient of determination ($R^2 = 0.99$):

$$565 \quad \varepsilon'_{container} = 1.419\varepsilon'_{sample} - 2.543 \quad (9)$$

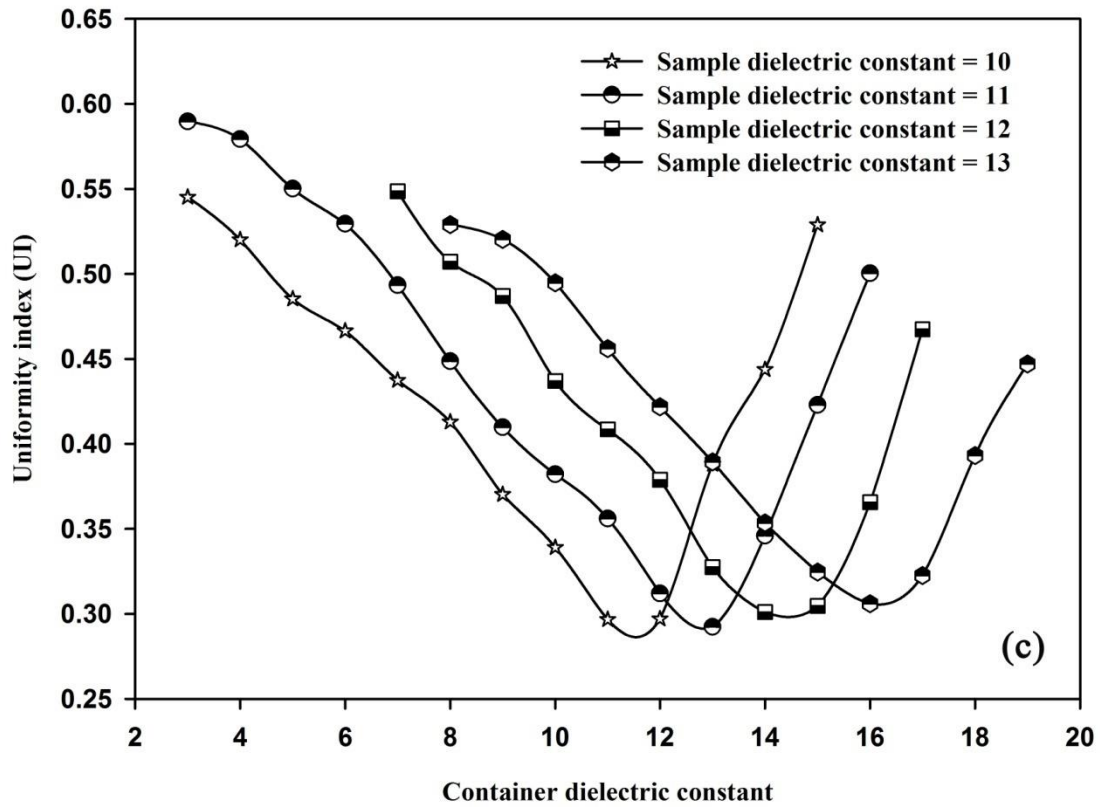
566 The predicted dielectric constant value of surrounding material was 8.8 with the DPs of
567 wheat flour fixed as $8-10*j$ based on the developed regression equation. There was little
568 difference with the literature findings that UI was the lowest when the surrounding material
569 dielectric constant was between 8 and 11 (Tiwari et al., 2011a). The calculated dielectric
570 constant value of surrounding sheets was 3.17 with DPs of peanut butter of $4.03-0.004*j$. This
571 was in good agreement with previous simulation results that the RF heating uniformity was
572 improved by using the PEI (DPs of $3.15-0.0025*j$) assisting method (Jiao et al., 2014a,
573 2015b). Obviously, results demonstrated that the developed correlation equation is reliable for
574 choosing the most suitable surrounding material to improve the RF heating uniformity in
575 various food products. For example, the estimated dielectric constant value of surrounding
576 container was 2.6 with dry soybeans DPs of $3.6-0.26*j$. This was in accordance with our
577 preliminary studies that UI was the lowest when the surrounding material dielectric constant
578 was between 2.5 and 3.5 (Huang et al., 2015c, 2016). Optimum RF heating uniformity in
579 other dry products (such as almond, lentil, wheat, walnut, pistachio nut, raisin, and rice) could
580 be achieved with a particular dielectric constant values of the surrounding material.



581



582



583

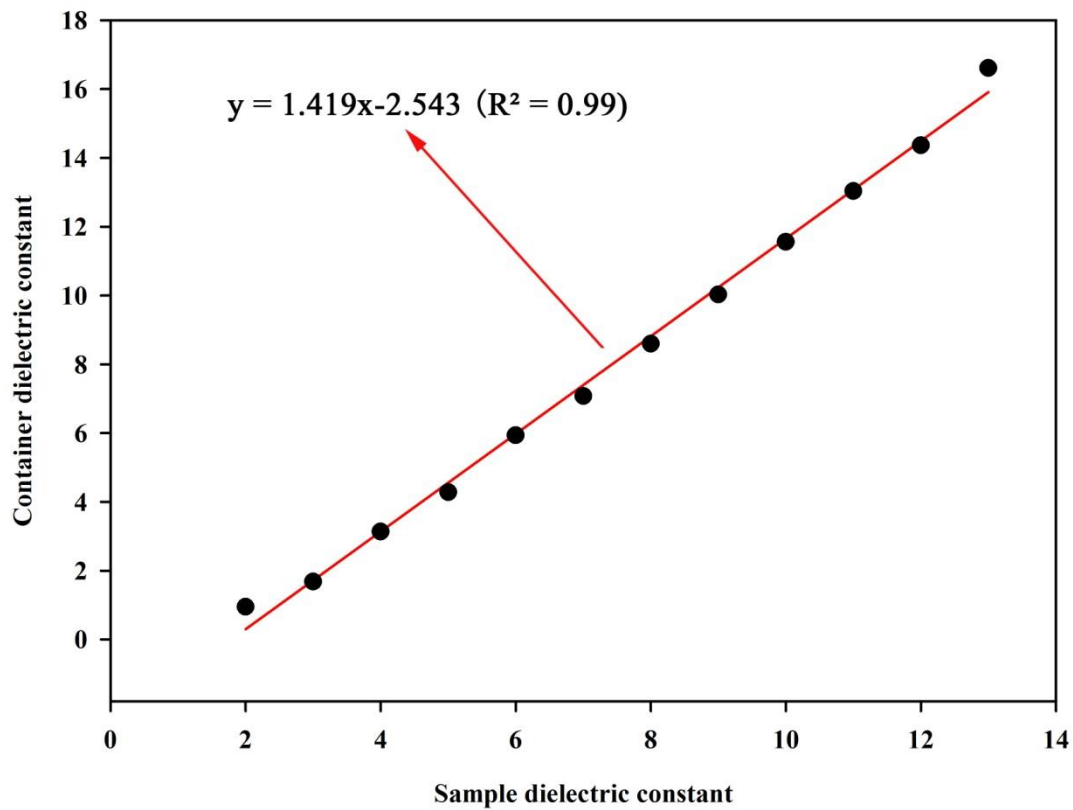
584 Fig. 12. Simulated UI of soybean flour with varying sample dielectric constants between (a)
 585 2-5, (b) 6-9, and (c) 10-13 under various container dielectric constants after 5 min RF heating
 586 with an electrode gap of 12 cm.

587 Table 5. The calculated dielectric constants of the surrounding container ($\epsilon'_{container}$) when the
 588 UI obtained the minimum values and the corresponding inputted voltages (V) with varying
 589 sample dielectric constants (ϵ'_{sample}) in each simulation after 5 min RF heating.

ϵ'_{sample}	2	3	4	5	6	7
$\epsilon'_{container}$	0.94	1.68	3.13	4.28	5.93	7.07
Simulation voltage (V)	2860	3540	4000	4490	5000	5600
ϵ'_{sample}	8	9	10	11	12	13

$\epsilon'_{container}$	8.59	10.03	11.56	13.03	14.36	16.61
Simulation voltage (V)	6280	6820	7430	8060	8630	9300

590



591

592 Fig. 13. Dielectric constant correlations between surrounding container and the treated food
 593 products when the simulated UI obtained the minimum values after 5 min heating time in a 12
 594 cm electrode gap.

595 3.6. Effect of loss factor of sample and container on sample UI

596 Table 6 compares the simulated UIs of soybean flour with different loss factor values of
 597 surrounding container and heated sample. UI showed a sharp decrease first and then a
 598 constant as a function of container loss factor. The UI decreased from 5.052 to 0.244 when
 599 loss factor of the surrounding container decreased from 0.3 to 0.00003 with the fixed sample
 600 loss factor of 0.1. It is also observed that when loss factor of sample increased gradually to 5,

601 UI decreased from 0.472 to 0.321. UI was the lowest compared to other loss factor values
 602 when loss factors of the surrounding container were given between 0.00003 and 0.0003,
 603 0.01-0.1% of the sample's one. Loss factor of sample describes the amount of electric energy
 604 converted to heat and the inputted voltages were lower when the sample loss factor decreased
 605 (Table 6). It is clear that the heating uniformity of food products could be improved when loss
 606 factors are small both for the surrounding container and treated samples (Huang et al, 2015b).
 607 The UI may not be further reduced due to the small enough loss factor values of the
 608 polystyrene container (0.0003) used in this study. Therefore, the dielectric constant of
 609 surrounding container is the dominating factor to influence the heating uniformity of treated
 610 products. This behaviour has been observed for dry soybeans (Huang et al., 2015c, 2016),
 611 peanut butter (Jiao et al., 2014a, 2015b), shell eggs (Lau, 2015), and wheat flour (Tiwari et al.,
 612 2011a) subjected to RF treatment.

613
 614 Table 6. Simulated UI of soybean flour with varying loss factor values of sample (ϵ''_{sample}) and
 615 surrounding container ($\epsilon''_{container}$) under the corresponding inputted voltages (V) after 5 min RF
 616 heating with an electrode gap of 12 cm.

ϵ''_{sample}	0.1					1				
	$\epsilon''_{container}$	0.3	0.03	0.003	0.0003	0.00003	0.3	0.03	0.003	0.0003
UI	5.052	0.584	0.278	0.247	0.244	0.616	0.286	0.245	0.242	0.241
Simulation voltage (V)	9150	8000	8000	8000	8000	2580	2570	2560	2560	2560
ϵ''_{sample}	3					5				
	$\epsilon''_{container}$	0.3	0.03	0.003	0.0003	0.00003	0.3	0.03	0.003	0.0003
UI	0.619	0.494	0.482	0.481	0.481	0.472	0.336	0.322	0.321	0.321

Simulation	1570	1570	1570	1570	1570	1670	1670	1670	1670	1670
voltage (V)										

617

618 3.7. Effect of density of sample and container on sample UI

619 Fig. 14 indicates that the smaller densities of surrounding container resulted in better RF
620 heating uniformities within the samples. UI decreased slightly with increasing densities of the
621 surrounding container but then increased dramatically under each fixed sample density values.
622 Low densities of the surrounding container should provide a better heating uniformity due to
623 the lower density values of heated material resulted in higher RF heating rate (Huang et al.,
624 2015b). Table 7 shows the calculated density values of surrounding container in each fixed
625 sample density when the minimum values of UI were obtained. The inputted voltage
626 increased with increasing sample density due to the positive correlation between sample
627 density and top electrode voltage (Birla et al., 2008). The general trend of density correlations
628 between the surrounding container and treated soybean flour was shown in Fig. 15 for
629 ensuring good RF heating uniformity. Therefore, a linear relationship for densities of
630 surrounding container and treated products was observed with high coefficient of
631 determination ($R^2=0.98$).

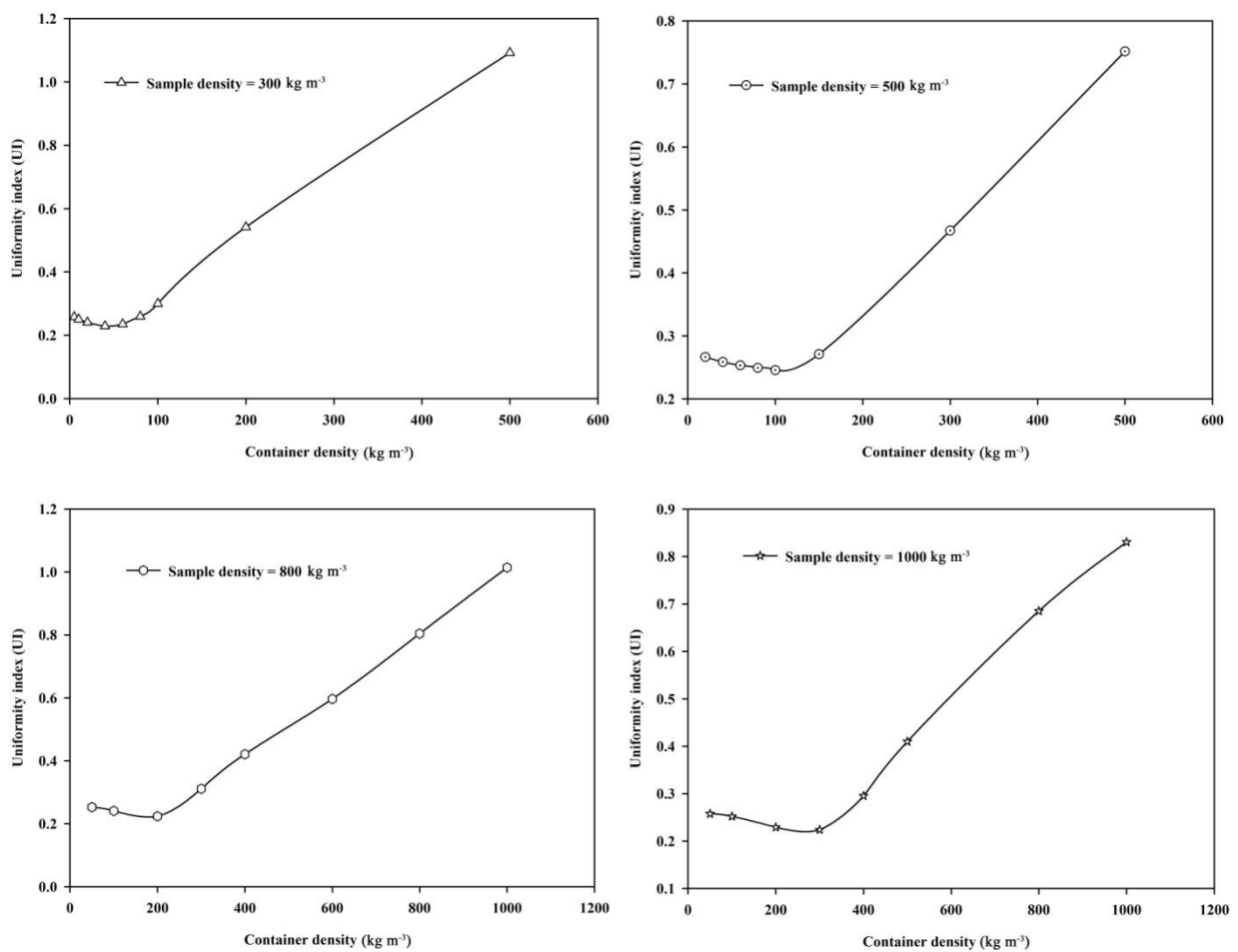
$$632 \quad \rho_{container} = 0.358\rho_{sample} - 68.10$$

633 (10)

634 It can be inferred from the above results that uniform RF heating of the sample could be
635 achieved when the surrounding container density was far small than the sample's one. The
636 regression equation developed in this study may be further used in other dry products and
637 other applications for heating uniformity improvement. Similar results have been also
638 obtained by Huang et al., (2016) that the temperature uniformity was greatly improved by
639 placing soybean samples in the polystyrene container (with low density) other than the

640 polypropylene container. This suggests that the developed relationship could possibly be
 641 applied to other low moisture foods for overcoming edge heating effect and maintaining good
 642 product quality. Therefore, in practical applications for an industrial-scale RF system, which
 643 was equipped with an auxiliary hot air system and conveyor belt, choosing an optimum
 644 container material could be effectively minimize the effect of electric field bending and
 645 distortion within the corners and edges of food products during the RF treatment. The
 646 developed correlation equations are a very effective tool for choosing the most suitable
 647 surrounding material to be used in an industrial application.

648

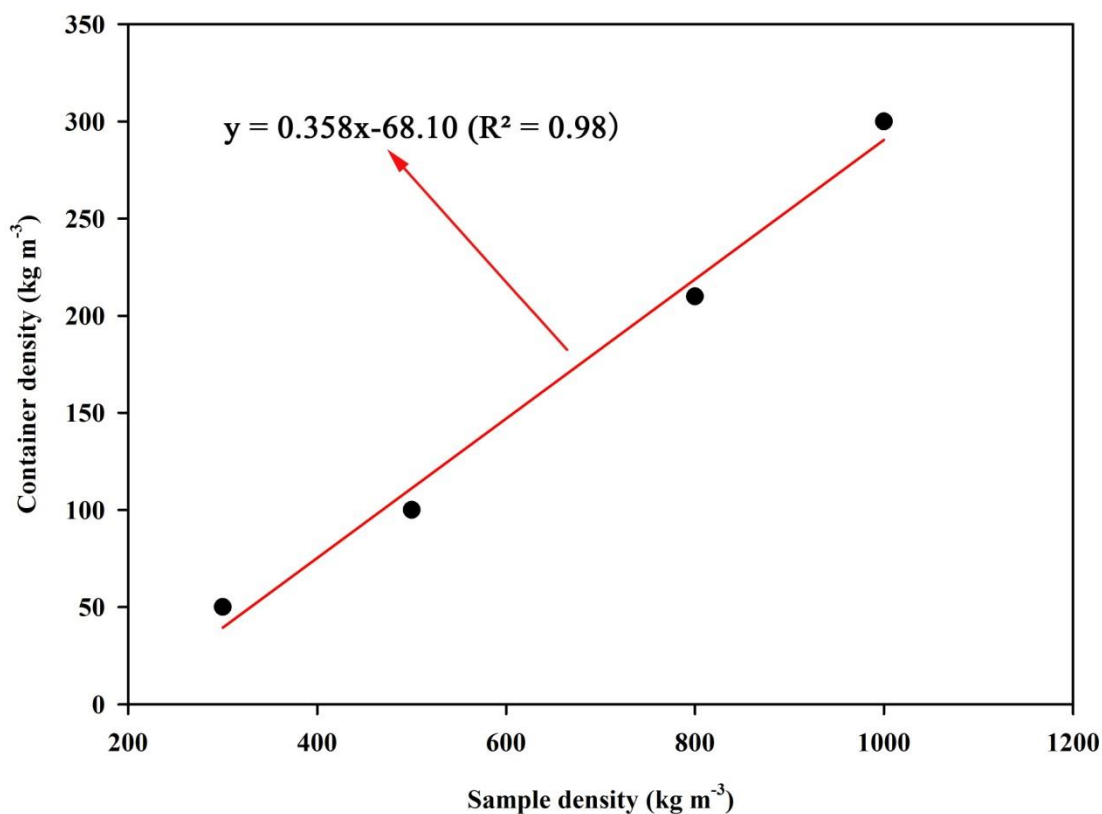


649 Fig. 14. Simulated UI of soybean flour with four different sample density values (300, 500,
 650 800, and 1000 kg m⁻³) and various container densities after 5 min RF heating with an
 651 electrode gap of 12 cm.

652 Table 7. The calculated density values of the surrounding container ($\rho_{container}$) when the UI
 653 obtained the minimum values and the corresponding inputted voltages (V) with varying
 654 sample densities (ρ_{sample}) in each simulation after 5 min RF heating.

Sample density (ρ_{sample} , kg m ⁻³)	300	500	800	1000
Container density ($\rho_{container}$, kg m ⁻³)	50	100	210	300
Simulation voltage (V)	3560	4620	5780	6460

655



656
 657 Fig. 15. Density correlations between the surrounding container and treated food products
 658 when the simulated UI obtained the minimum values after 5 min heating time in a 12 cm
 659 electrode gap.

660 **4. Conclusions**

661 A comprehensive coupled electromagnetic and heat transfer model was developed
662 considering quasi-static electric fields in a 6 kW, 27.12 MHz RF heating system. Simulated
663 temperature distribution in three horizontal layers of soybean flour were found in good
664 agreement with experimental temperature profiles, except for some corners with maximum
665 difference of 5 °C. The validated model was further used to study the effects of DPs and
666 density of sample and surrounding container on sample UI. Simulated results illustrated that
667 the RF heating uniformity could be improved when the dielectric constant and density of
668 surrounding container and sample were in accordance with the established relationships. The
669 smaller loss factor values for both surrounding container and heated products provided better
670 temperature uniformities. The obtained regression equations may be useful to obtain a better
671 heating uniformity in disinfestations of dry products and for designing an RF treatment
672 protocols.

673 **Acknowledgements**

674 This research was conducted in the College of Mechanical and Electronic Engineering,
675 Northwest A&F University, and supported by research grants from General Program of
676 National Natural Science Foundation of China (31371853) and Program of Introducing
677 International Advanced Agricultural Science and Technologies (948 Program) of Ministry of
678 Agriculture of China (2014-Z21). The authors thank Qian Hao, Hongxue Zhou, Rui Li,
679 Xiaoxi Kou, and Lixia Hou for their helps in conducting experiments.

680 **References**

- 681 AOAC. (2002). Official methods of analysis. Gaithersburg, MD, USA: Association of Official Analytical
682 Chemists.
- 683 Alfaifi, B., Tang, J., Jiao, Y., Wang, S., Rasco, B., Jiao, S., & Sablani, S. (2014). Radio frequency disinfestation
684 treatments for dried fruit: Model development and validation. *Journal of Food Engineering*, *120*,
685 268-276.
- 686 Ben-Lalli, A., Bohuon, P., Collignan, A., & Méot, J. M. (2013). Modeling heat transfer for disinfestation and
687 control of insects (larvae and eggs) in date fruits. *Journal of Food Engineering*, *116*(2), 505-514.
- 688 Birla, S., Wang, S., & Tang, J. (2008). Computer simulation of radio frequency heating of model fruit immersed
689 in water. *Journal of Food Engineering*, *84*(2), 270-280.
- 690 Birla, S., Wang, S., Tang, J., & Hallman, G. (2004). Improving heating uniformity of fresh fruit in radio
691 frequency treatments for pest control. *Postharvest Biology and Technology*, *33*(2), 205-217.

692 Chen, L., Wang, K., Li, W., & Wang, S. (2015a). A strategy to simulate radio frequency heating under mixing
693 conditions. *Computers and Electronics in Agriculture*, *118*, 100-110.

694 Chen, L., Huang, Z., Wang, K., Li, W., & Wang, S. (2015b). Simulation and validation of radio frequency
695 heating with conveyor movement. *Journal of Electromagnetic Waves and Applications*, in proof.

696 Choi, C., & Konrad, A. (1991). Finite element modeling of the RF heating process. *IEEE Trans. Magnetics*,
697 *27*(5), 4227-4230.

698 COMSOL material library, COMSOL Multiphysics, V4.3a, (2012). Burlington, MA, USA.

699 FAOSTAT. (2013) Food and Agriculture Organization of the United Nations. (Available at:[http://faostat.fao.org/
700 site/312/default.aspx](http://faostat.fao.org/site/312/default.aspx)).

701 Finn, S., Hinton, J. C., McClure, P., Amézquita, A., Martins, M., & Fanning, S. (2013). Phenotypic
702 characterization of salmonella isolated from food production environments associated with low-water
703 activity foods. *Journal of Food Protection*, *76*(9), 1488-1499.

704 Farag, K. W., Marra, F., Lyng, J. G., Morgan, D. J., & Cronin, D. A. (2010). Temperature changes and power
705 consumption during radio frequency tempering of beef lean/fat formulations. *Food and Bioprocess
706 Technology*, *3*(5), 732-740.

707 Fu, Y. C. (2004). Fundamentals and industrial applications of microwave and radio frequency in food processing.
708 *Food Processing: Principles and Applications*, Blackwell, Iowa, USA, pp. 79-100.

709 Gao, M., Tang, J., Villa-Rojas, R., Wang, Y., & Wang, S. (2011). Pasteurization process development for
710 controlling Salmonella in in-shell almonds using radio frequency energy. *Journal of Food Engineering*,
711 *104*(2), 299-306.

712 Geveke, D. J., Kozempel, M., Scullen, O. J., & Brunkhorst, C. (2002). Radio frequency energy effects on
713 microorganisms in foods. *Innovative Food Science and Emerging Technologies*, *3*, 133-138.

714 Guo, W., Wang, S., Tiwari, G., Johnson, J. A., & Tang, J. (2010). Temperature and moisture dependent
715 dielectric properties of legume flour associated with dielectric heating. *LWT-Food Science and
716 Technology*, *43*(2), 193-201.

717 Ha, J. W., Kim, S. Y., Ryu, S. R., & Kang, D. H. (2013). Inactivation of Salmonella enterica serovar
718 Typhimurium and Escherichia coli O157: H7 in peanut butter cracker sandwiches by radio-frequency
719 heating. *Food Microbiology*, *34*(1), 145-150.

720 Hassan, S. M. (2013). *Soybean, Nutrition and Health-Chapter 20*. Intech open access publisher. Rijeka, Croatia,
721 European Union, pp. 453-473.

722 Hou, L., Ling, B., & Wang, S. (2014). Development of thermal treatment protocol for disinfesting chestnuts
723 using radio frequency energy. *Postharvest Biology and Technology*, *98*, 65-71.

724 Huang, Z., Chen, L., & Wang, S. (2015a). Computer simulation of radio frequency selective heating of insects in
725 soybeans. *International Journal of Heat and Mass Transfer*, *90*, 406-417.

726 Huang, Z., Zhu, H., & Wang, S. (2015b). Finite element modelling and analysis of radio frequency heating rate
727 in mung beans. *Transactions of the ASABE*, *58*(1), 149-160.

728 Huang, Z., Zhu, H., Yan, R., & Wang, S. (2015c). Simulation and prediction of radio frequency heating in dry
729 soybeans. *Biosystems Engineering*, *129*, 34-47.

730 Huang, Z., Zhang, B., Marra F., & Wang, S. (2016). Computational modelling of the impact of polystyrene
731 containers on radio frequency heating uniformity improvement for dried soybeans. *Innovative Food
732 Science and Emerging Technologies*, accepted.

733 Ikediala, J., Hansen, J., Tang, J., Drake, S., & Wang, S. (2002). Development of a saline water immersion
734 technique with RF energy as a postharvest treatment against codling moth in cherries. *Postharvest
735 Biology and Technology*, *24*(2), 209-221.

736 Jiao, S., Deng, Y., Zhong, Y., Wang, D., & Zhao, Y. (2015a). Investigation of radio frequency heating
737 uniformity of wheat kernels by using the developed computer simulation model. *Food Research
738 International*, *71*, 41-49.

739 Jiao, S., Johnson, J., Tang, J., & Wang, S. (2012). Industrial-scale radio frequency treatments for insect control
740 in lentils. *Journal of Stored Products Research*, *48*, 143-148.

741 Jiao, Y., Shi, H., Tang, J., Li, F., & Wang, S. (2015b). Improvement of radio frequency (RF) heating uniformity
742 on low moisture foods with Polyetherimide (PEI) blocks. *Food Research International*, *74*, 106-114.

743 Jiao, Y., Tang, J., & Wang, S. (2014a). A new strategy to improve heating uniformity of low moisture foods in
744 radio frequency treatment for pathogen control. *Journal of Food Engineering*, *141*, 128-138.

745 Jiao, Y., Tang, J., Wang, S., & Koral, T. (2014b). Influence of dielectric properties on the heating rate in
746 free-running oscillator radio frequency systems. *Journal of Food Engineering*, *120*, 197-203.

747 Johnson, J., Wang, S., & Tang, J. (2003). Thermal death kinetics of fifth-instar *Plodia interpunctella*
748 (Lepidoptera: Pyralidae). *Journal of Economic Entomology*, *96*(2), 519-524.

749 Johnson, J., Wang, S., & Tang, J. (2010). Radio frequency treatments for insect disinfestation of dried legumes.
750 In *Proc.10th Intl. Working Conf. Stored Product Protection* (pp. 688-694), Berlin, Germany: Julius
751 Kühn Institut.

752 Kim, S. Y., Sagong, H. G., Choi, S. H., Ryu, S., & Kang, D. H. (2012). Radio-frequency heating to inactivate
753 *Salmonella Typhimurium* and *Escherichia coli O157: H7* on black and red pepper spice. *International*
754 *Journal of Food Microbiology*, 153(1), 171-175.

755 Kirmaci, B., & Singh, R. K. (2012). Quality of chicken breast meat cooked in a pilot-scale radio frequency oven.
756 *Innovative Food Science and Emerging Technologies*, 14, 77-84.

757 Lau, S. K. (2015). Simulation and validation of radio frequency heating of shell eggs. *Dissertations & Theses in*
758 *Food Science and Technology*, 61, 1-133.

759 Liu, Y., Wang, S., Mao, Z., Tang, J., & Tiwari, G. (2013). Heating patterns of white bread loaf in combined
760 radio frequency and hot air treatment. *Journal of Food Engineering*, 116(2), 472-477.

761 Llave, Y., Liu, S., Fukuoka, M., & Sakai, N. (2015). Computer simulation of radiofrequency defrosting of frozen
762 foods. *Journal of Food Engineering*, 152, 32-42.

763 Luechapattanaorn, K., Wang, Y., Wang, J., Tang, J., Hallberg, L. M., & Dunne, C. P. (2005). Sterilization of
764 scrambled eggs in military polymeric trays by radio frequency energy. *Journal of Food Science*, 70(4),
765 288-294.

766 Marra, F., Lyng, J., Romano, V., & McKenna, B. (2007). Radio-frequency heating of foodstuff: Solution and
767 validation of a mathematical model. *Journal of Food Engineering*, 79(3), 998-1006.

768 Marshall, M., & Metaxas, A. (1998). Modeling of the radio frequency electric field strength developed during
769 the RF assisted heat pump drying of particulates. *Journal of Microwave Power and Electromagnetic*
770 *Energy*, 33(3), 167-177.

771 Metaxas, A. (1996). *Foundations of electroheat: a unified approach*. John Wiley & Sons, New York.

772 Mitcham, E., Veltman, R., Feng, X., De Castro, E., Johnson, J., Simpson, T., Biasi, W., Wang, S., & Tang, J.
773 (2004). Application of radio frequency treatments to control insects in in-shell walnuts. *Postharvest*
774 *Biology and Technology*, 33(1), 93-100.

775 Mohapatra, D., Kar, A., & Giri, S. K. (2015). Insect pest management in stored pulses: an overview. *Food and*
776 *Bioprocess Technology*, 8(2), 239-265.

777 Shrestha, B., & Baik, O. D. (2013). Radio frequency selective heating of stored-grain insects at 27.12 MHz: a
778 feasibility study. *Biosystems Engineering*, 114(3), 195-204.

779 Singh, P., Satya, S., & Naik, S. (2013). Grain Storage insect-pest infestation-issues related to food quality and
780 safety. *Internet Journal of Food Safety*, 15, 64-73.

781 Taylor, W. G., Fields, P. G., & Sutherland, D. H. (2007). Fractionation of lentil seeds (*lens culinaris medik.*) for
782 insecticidal and flavonol tetraglycoside components. *Journal of Agricultural and Food Chemistry*,
783 55(14), 5491-5498.

784 Tiwari, G., Wang, S., Tang, J., & Birla, S. (2011a). Analysis of radio frequency (RF) power distribution in dry
785 food materials. *Journal of Food Engineering*, 104(4), 548-556.

786 Tiwari, G., Wang, S., Tang, J., & Birla, S. (2011b). Computer simulation model development and validation for
787 radio frequency (RF) heating of dry food materials. *Journal of Food Engineering*, 105(1), 48-55.

788 Uyar, R., Bedane, T. F., Erdogdu, F., Palazoglu, T. K., Farag, K. W., & Marra, F. (2015). Radio-frequency
789 thawing of food products—A computational study. *Journal of Food Engineering*, 146, 163-171.

790 Vijay, S., Bhuvaneshwari, K., & Gajendran, G. (2015). Assessment of grain damage and weight loss caused by
791 *Sitophilus oryzae (L.)* feeding on split pulses. *Agricultural Science Digest*, 35(2), 111-115.

792 Wang, S., Monzon, M., Johnson, J., Mitcham, E., & Tang, J. (2007). Industrial-scale radio frequency treatments
793 for insect control in walnuts: I: Heating uniformity and energy efficiency. *Postharvest Biology and*
794 *Technology*, 45(2), 240-246.

795 Wang, S., Tiwari, G., Jiao, S., Johnson, J., & Tang, J. (2010). Developing postharvest disinfestation treatments
796 for legumes using radio frequency energy. *Biosystems Engineering*, 105(3), 341-349.

797 Wang, S., Yue, J., Chen, B., & Tang, J. (2008). Treatment design of radio frequency heating based on insect
798 control and product quality. *Postharvest Biology and Technology*, 49(3), 417-423.

799 Wang, S., Yue, J., Tang, J., & Chen, B. (2005). Mathematical modelling of heating uniformity for in-shell
800 walnuts subjected to radio frequency treatments with intermittent stirrings. *Postharvest Biology and*
801 *Technology*, 35(1), 97-107.

802 Zhu, H., Huang, Z., & Wang, S. (2014). Experimental and simulated top electrode voltage in free-running
803 oscillator radio frequency systems. *Journal of Electromagnetic Waves and Applications*, 28(5),
804 606-617.

805